TITLE

Divergence of cytokinesis and dimorphism control by myosin II regulatory light chain in fission yeasts

Running title

Evolutionary regulation of cytokinesis and dimorphism in fission yeasts.

AUTHORS AND AFFILIATIONS

Francisco Prieto-Ruiz[1], Elisa Gómez-Gil[2], Jero Vicente-Soler[1], Alejandro Franco[1], Teresa Soto[1], Marisa Madrid[1]*, José Cansado[1]*#

[1]Yeast Physiology Group. Department of Genetics and Microbiology. Campus de Excelencia Internacional de Ámbito Regional (CEIR) Campus Mare Nostrum, Universidad de Murcia. 30071 Murcia, Spain.

[2]The Francis Crick Institute, 1 Midland Road, London, NW1 1AT, UK.

* To whom correspondence should be addressed:

José Cansado, jcansado@um.es

Marisa Madrid, marisa@um.es

Lead contact

SUMMARY

Non-muscle myosin II activation by regulatory light chain (Rlc1^{Sp}) phosphorylation at Ser35 is crucial for cytokinesis during respiration in the fission yeast *Schizosaccharomyces pombe*. We show that in the early divergent and dimorphic fission yeast *S. japonicus* non-phosphorylated Rlc1^{Sj} regulates the activity of Myo2^{Sj} and Myp2^{Sj} heavy chains during cytokinesis. Intriguingly, Rlc1^{Sj}-Myo2^{Sj} nodes delay yeast to hyphae onset but are essential for mycelial development. Structure-function analysis revealed that phosphorylation-induced folding of Rlc1^{Sp} α1 helix into an open conformation allows precise regulation of Myo2^{Sp} during cytokinesis. Consistently, inclusion of bulky tryptophan residues in the adjacent α5 helix triggered Rlc1^{Sp} shift and supported cytokinesis in absence of Ser35 phosphorylation. Remarkably, unphosphorylated Rlc1^{Sj} lacking the α1 helix was competent to regulate *S. pombe* cytokinesis during respiration. Hence, early diversification resulted in two efficient phosphorylation-independent and -dependent modes of Rlc1 regulation of myosin II activity in fission yeasts, the latter being conserved through evolution.

INTRODUCTION

Non-muscle myosin II (NMII), a member of the myosin superfamily of molecular motors, is an actin-based multimeric protein complex that generates most of the mechanical force in eukaryotes to regulate essential processes such as cell migration, division and cytokinesis [1]. In animal cells, NMII is assembled from two heavy chains, two essential light chains (ELC), and two regulatory light chains (RLC), which control the function of the multimer by promoting its folding into an active conformation in response to phosphorylation [1]. Phosphorylation of RLC at Ser19 is essential for NMII activation, leading to the formation of bipolar filaments with increased actin binding affinity and ATPase motor activity [1-3].

NMII orthologs also play important roles in the fungal kingdom. They control septation, development, and virulence in plant and human filamentous fungi [4-8], and are key modulators of cytokinesis in both budding and fission yeasts [9-12]. The fission yeast *Schizosaccharomyces pombe*, one of four species within the genus *Schizosaccharomyces*, a monophyletic clade of the phylum *Ascomycota*, is a well-established model organism for studying of the spatiotemporal regulation of cytokinesis during symmetric cell division [9-13]. Early in metaphase *S. pombe* cells assemble a centrally positioned actomyosin ring ('CAR') from nodes composed of actin filaments and myosin II, which provides the mechanical force for actomyosin contractility [9-13]. The two myosin-II heavy chains Myo2 and Myp2/Myo3 (hereafter Myo2^{Sp} and Myp2^{Sp}) are involved in CAR assembly and closure in *S. pombe* [12]. Myo2^{Sp} is essential for cytokinesis and cell viability, whereas Myp2^{Sp} function is not essential but cooperates with Myo2^{Sp} during CAR closure and in response to salt stress [14-16]. Rlc1^{Sp}, the RLC shared by Myo2^{Sp} and Myp2^{Sp} [17,18], is phosphorylated *in vivo* at Ser35 within its N-terminus [19-21]. Interestingly, we have recently shown that Rlc1^{Sp} phosphorylation is not biologically relevant during fermentative growth in the presence of glucose, but becomes essential to modulate Myo2^{Sp} activity during cytokinesis when *S. pombe* grows under respiratory metabolism [22]. The p21/Cdc42-activated kinase (PAK) Pak1, either alone or in combination with Pak2, a second PAK ortholog, is responsible for the *in vivo* phosphorylation of Rlc1^{Sp} at Ser35 during fermentation and respiration, respectively [20,22].

The fission yeast *S. japonicus* forms an early divergent branch from *S. pombe* and the remaining *Schizosaccharomyces* species *S. octosporus* and *S. cryophilus* [23,24]. Despite the high number of shared gene orthologs and conserved cellular processes, *S. japonicus* yeast cells exhibit important and distinctive physiological features with respect to *S. pombe*, including a semi-open mitosis [25-28], the absence of a respiratory

metabolism [29], and the ability to develop a robust differentiation into hyphae in response to environmental cues and DNA damage [24,30-33]. In addition, in *S. japonicus* Myo2^{Sj} and Rlc1^{Sj} are targeted to nodes at the equatorial cortex during interphase early in G2, and, in contrast to *S. pombe*, the assembly of a mature CAR occurs late in anaphase during exit from mitosis [13,34].

Here, we comparatively explored the biological significance and evolutionary conservation of Rlc1 and myosin II function during cytokinesis and yeast-to-hypha dimorphism in *S. japonicus* and *S. pombe.* We found that non-phosphorylated Rlc1^{Sj} regulates CAR assembly and closure in *S. japonicus* through heavy chains Myo2^{Sj} and Myp2^{Sj}, while the Rlc1^{Sj}-Myo2^{Sj} pair specifically repress the early stages of hyphal differentiation but is essential for efficient myceliation. *In vivo* phosphorylation of Rlc1^{Sp} at Ser35 induces a N-terminal shift to an open conformation that is essential to control cytokinetic Myo2^{Sp} activity during respiration, thus supporting the proposed mechanism for RLC activation in animal cells. Surprisingly Rlc1^{Sj}, which lacks the α helix and the phosphorylation site, fully supported Myo2^{Sp} function during *S. pombe* respiration, suggesting that Rlc1 functionality is intrinsically linked to its open conformation.

RESULTS

Regulation of cytokinesis by myosin II light chain Rlc1 in *S. japonicus*.

Rlc1^{Sp} has a high overall amino-acid sequence identity (~76%) with Rlc1^{So} and Rlc1^{Sc}, the respective *S. octosporus* and *S. cryophilus* orthologs (Figure 1A). Amino-acid conservation is significantly reduced when compared to *S. japonicus* Rlc1^{Sj} (~56%), particularly in their respective N-terminal domains (Figure 1A). Rlc1^{Sp} has a long N-terminal tail followed by a serine residue at position 35 (-KRA<u>S</u>S- sequence), which is phosphorylated *in vivo* by the p21-activated kinases Pak1 and Pak2 (Figure 1A) [20,22]. In contrast, Rlc1^{Sj} lacks 12 amino acids of this N-terminal motif and the putative PAK-phosphorylation site, which is replaced by an asparagine at position 23 (sequence –KRI<u>N</u>S-) (Figure 1A). These structural differences prompted us to investigate the evolutionary conservation of Rlc1 and myosin II function in the two distant fission yeasts.

Rlc1^{Sj} forms an equatorial band of cortical nodes in interphase that condense into the CAR late in anaphase at the mitotic exit [34], as evidenced by microscopy time-lapse analysis of cells co-expressing genomic mCherry fusions of Rlc1^{Sj} and Pcp1, a pericentrin SPB component as an internal control for mitotic progression (Figure 1B). Like the *S. pombe rlc1*Δ mutant [17,18], *S. japonicus rlc1*Δ cells accumulated a

significant number of multiseptated cells at the stationary phase of cell growth, often with thickened and incomplete septa, suggesting a cytokinetic defect (Figure 1C). *S. japonicus rlc1*Δ cells were also growth-sensitive and multiseptated when incubated at high temperature (37-42ºC) or with 1-1.2M KCl (Figure 1C, 1D). We performed a comparative time-lapse fluorescence microscopy analysis of CAR dynamics in wild-type and *rlc1*Δ cells co-expressing genomic fusions of Pcp1-mCherry and Cdc15-GFP, an F-BAR protein that localizes to the CAR during cytokinesis [34]. The total time for ring assembly and constriction in *rlc1*Δ cells was substantially longer than in wild-type cells (56.88 ± 7.97 *vs* 46 ± 4.04 min, respectively) (Figure 1E, 1F). The cytokinetic delay was observed in both the stages of ring maturation (35.22 ± 2.82 *vs* 29.64 ± 2.41 min, respectively) and ring closure and disassembly (21.66 ± 6.92 *vs* 16.36 ± 2.99 min, respectively), together with a slower constriction rate (0.803 ± 0.02 *vs* 0.626 + 0.02 μm/min, respectively) (Figure 1E, 1F). Thus, like the *S. pombe* ortholog, Rlc1^{Sj} plays a significant and positive regulatory role of myosin II during cytokinesis in *S. japonicus*.

Rlc1^{Sj} negatively regulates the early stages of the dimorphic switch in *S. japonicus* but is required for myceliation.

S. japonicus yeast cells undergo a strong dimorphic switch to hyphae when grown in low nitrogen solid media (YEMA) or supplemented with red grape extract (RGE) [32,33]. Under these conditions, yeast cells first transform into transition forms (monopolar growing cells with numerous small vacuoles at the non-growing end), which eventually develop into hyphae (large monopolar growing cells with 1-2 large vacuoles at the non-growing end) [30,33]. Compared to the wild-type, *rlc1*Δ cells developed into transition forms and hyphae earlier during incubation on RGE-agarose pads (Figure 2A) or after 3 and 6h of incubation in liquid culture with 0.2 μM camptotecin (CPT), which triggers rapid hyphal differentiation without inducing a checkpoint arrest (Figure 2B) [35].

Rlc1^{Sj} localized to the equatorial cortex as a few dispersed nodes in transition forms and hyphae during CPT treatment and was never observed at the cell poles (Figure S1A). Hyphal development in *S. japonicus* is strongly dependent on vesicle transport on actin cables for polarized growth [33]. Image segmentation analysis of CPT-treated cells immunostained with AlexaFluor-488-phalloidin using the machine learning routine Ilastik [36], showed that the actin cable-to-patch ratio did not change significantly in yeasts,

transition forms, and hyphae in wild-type *versus rlc1*Δ cells (Figure S1B). Remarkably, the average growth rate of transition forms was almost identical in wild-type and *rlc1*Δ cells during hyphal induction in RGE-agarose pads (Figure 2A).

In contrast, mycelial expansion of the *rlc1*Δ mutant was significantly reduced with respect to the wild type after seven days of incubation in YEMA and RGE solid media (Figure 2C). We compared the differentiation of hyphae isolated from wild-type and *rlc1*Δ mycelia incubated in semi-solid RGE medium with gelatin instead of agar (Figure 2D) [37]. Calcofluor staining revealed that *rlc1*Δ hyphae recovered from 10-days-old mycelia were significantly shorter and accumulated a high number of thickened and incomplete septa as compared to the wild type (Figure 2D, 2E). Collectively, this evidence supports that regulation of myosin II activity by Rlc1^{Sj} has a negative impact on the early stages of *S. japonicus* yeast to hyphae transition, whereas its function is positive and necessary for a robust mycelium development.

Distinctive roles of the myosin-II heavy chains Myo2 and Myp2 during cytokinesis and dimorphism in *S. japonicus*.

Rlc1^{Sp} is the RLC for the two myosin-II heavy chains Myo2 and Myp2/Myo3 [17,18,38]. The *S. japonicus* proteome also carries two putative orthologs, Myo2^{Sj} (SJAG_03703) and Myp2^{Sj}/Myo3^{Sj} (SJAG_02431), which share ~54 and ~44% total sequence identity with their *S. pombe* counterparts, respectively. Similar to the *S. pombe* myosins [12], Myo2^{Sj} and Myp2^{Sj} possess the conserved motor domains plus ATP, actin-binding sites, and the IQ motifs that define the binding sites for ELC and RLC (Figure S2A). Myp2^{Sj} also has highly disrupted coiled-coil regions within its long tail, which is slightly shorter than Myp2^{Sp} (Figure S2A). Similar to Rlc1^{Sj}, Myo2^{Sj} forms an equatorial band of cortical nodes during interphase that condenses into the CAR late in anaphase, as confirmed by microscopic time-lapse analysis of GFP-Myo2^{Sj} and Pcp1^{Sj}-mCherry fusions (Figure S2B) [34]. As in *S. pombe*, a Myp2^{Sj}-GFP fusion co-localized with Rlc1^{Sj} -mCherry late after CAR condensation and remained until the stage of ring closure (Figure 3A). Thus, the dynamics of myosin II heavy chains Myo2 and Myp2 and Rlc1 targeting to the CAR during cytokinesis are conserved in both fission yeast species.

Repeated attempts to obtain an *S. japonicus* mutant lacking Myo2^{Sj} were unsuccessful, suggesting that, as in *S. pombe*, its function is essential for cell growth. Indeed, we found that *S. japonicus* cells

expressing the N-terminal GFP-Myo2^{Sj} version are hypomorphic for Myo2 function, and exhibit phenotypes like those associated with Rlc1 deletion (Figure 1C, 1D), including growth sensitivity at elevated temperatures or in the presence of salt (Figure 3B) and multiseptation (Figure 3C). Accordingly, GFP-Myo2 cells exhibited much longer times for ring maturation (34.44 ± 3.04 *vs.* 27.13 ± 2.26 min, respectively), ring closure and disassembly (31.78 ± 2.39 *vs.* 13.81 ± 1.46 min), and slower constriction rate (0.584 ± 0.01 *vs.* 0.980 ± 0.02 μm/min) compared to wild-type cells (Figure 3D, 3E).

Myp2^{Sp} is not essential in *S. pombe*, but it plays an important role in CAR closure during unperturbed growth and in response to salt stress [16]. *S. japonicus myp2*Δ cells were salt sensitive for growth like the *rlc1*Δ mutant (Figure 3B). They showed a specific cytokinetic delay in ring closure (21.68 ± 2.73 *vs.* 13.81 ± 1.46 min) and a subsequent reduction in the rate of ring constriction (0.785 ± 0.02 *vs.* 0.980 ± 0.02 μm/min) (Figure 3D, 3E) and multiseptation (Figure 3C). These results suggest that Rlc1-dependent control of the two myosin-II heavy chains, Myo2 and Myp2, is biologically relevant for cytokinesis in *S. japonicus* during vegetative growth and stress.

Similar to the *rlc1*Δ mutant (Figure 2A-2C), and in contrast to wild-type and *myp2*Δ cells, GFP-Myo2^{Sj} cells rapidly developed into monopolar transition forms during incubation in RGE pads or after treatment with CPT in liquid culture (Figure 3F; Figure S2C). *S. japonicus* Myo2^{Sj} and Rlc1^{Sj} are targeted to nodes in the equatorial cortex early in G2 by the medial ring protein Mid1, and this localization pattern is lost in *mid1*Δ cells [34]. However, the recruitment of Myo2^{Sj} and Rlc1^{Sj} for medial CAR assembly during cytokinesis is not mediated by Mid1 [34]. Remarkably, differentiation of yeast cells into monopolar transition forms was also faster in a *mid1*Δ mutant and in *mid1*Δ cells expressing a Mid1^{Sp} version that remains localized to the nucleus during interphase and is redistributed to the lateral cortex early in mitosis (Figure 3F) [10,34]. Again, the average growth rate of transition forms did not change significantly between wild-type, GFP-Myo2^{Sj}, *myp2*Δ, *mid1*Δ and Mid1^{Sp} cells during hyphal induction (Figure S2D). Taken together, these observations suggest that interphase Myo2^{Sj} and Rlc1^{Sj} nodes in the equatorial cortex negatively regulate the early stages of yeast to hypha differentiation in *S. japonicus*.

Finally, mycelial expansion of GFP-Myo2^{Sj} cells in either YEMA or RGB media was reduced to a similar extent as in *rlc1*Δ cells, whereas *myp2*Δ, *mid1*Δ and Mid1^{Sp} mutants showed an identical ability to develop mycelium as wild-type cells (Figure 3G, 3H). Like *rlc1*Δ hyphae, GFP-Myo2^{Sj} hyphae recovered

from RGE-plates also accumulated a high number of septa compared to the wild type (Figure S2E). Therefore, the Rlc1^{Sj} -Myo2^{Sj} association is essential for late hyphal differentiation and mycelia formation.

In vivo phosphorylation of Rlc1 negatively affects Myo2 function in _S. japonicus_ during cytokinesis and myceliation.

The divergence between the N-terminal sequences of Rlc1^{Sj} and Rlc1^{Sp}, as well as the absence of a putative Pak1-phoshorylation site in Rlc1^{Sj}, led us to investigate the evolutionary impact of these changes on the regulation of myosin II function in the two species. To this end, we generated *S. japonicus rlc1*Δ mutants expressing different genomic wild-type and mutant constructs of Rlc1^{Sj} and Rlc1^{Sp} fused to GFP under the control of their respective wild-type promoters. We then asked what effect restoring the *in vivo* phosphorylation of Rlc1^{Sj} might have on myosin II functions in this species. We used site-directed mutagenesis to generate an Rlc1^{Sj} version in which Asn23, equivalent to Rlc1^{Sp} Ser35, was replaced by a phosphorylatable serine residue (Rlc1^{Sj} (N23S)-GFP fusion). Rlc1^{Sj} (N23S)-GFP was phosphorylated at this residue *in vivo*, as confirmed by the appearance of a slower motility band on Phos-tag SDS-PAGE, which is absent in wild-type Rlc1^{Sj}-GFP (Figure 4A). Rlc1^{Sj} (N23S)-GFP cells grew normally in rich medium at standard temperature (28-30ºC) or in medium supplemented with 1-1.2M KCl but were slightly thermosensitive at 40ºC (Figure 4B). Accordingly, they showed a modest but significant cytokinetic delay during the ring closure and disassembly phase, with a slower rate of ring constriction when incubated at 37ºC (Figure 4C, 4D). This resulted in a marked increase in the number of septated and multiseptated cells, and very similar to that seen in the *rlc1*Δ mutant (Figure S3). Importantly, *in vivo* phosphorylation of Rlc1^{Sj} at S23 resulted in premature development of yeasts into monopolar transition forms (Figure 4E) and was detrimental to *S. japonicus* myceliation in solid media to a similar extent as in *rlc1*Δ cells (Figure 4F, 4G).

A Rlc1^{Sp}-GFP fusion expressed in *S. japonicus rlc1*Δ cells is phosphorylated at Ser35 *in vivo* as in *S. pombe* (Figure 4A). Remarkably, *S. japonicus* Rlc1^{Sp}-GFP cells phenocopied those expressing the phosphorylated Rlc1^{Sj} (N23S)-GFP version, as they were partially thermosensitive (Figure 4B), showed a delay in ring constriction and reduced constriction rates during cytokinesis (Figure 4C, 4D), and accumulated septated/multiseptated cells at high temperature (Figure S3). They also differentiated more rapidly into transition forms (Figure 4E) and were defective for long-term mycelial development in YEMA and RGE

plates (Figure 4F, 4G). Most importantly, these phenotypes were completely suppressed when Ser35 was replaced by a non-phosphorylatable alanine residue (Rlc1^{Sp} (S35A)-GFP mutant) (Figure 4B-4F). Altogether, our results indicate that PAK-dependent *in vivo* phosphorylation negatively affects Rlc1^{Sj} regulation of myosin II function in *S. japonicus* during cytokinesis and yeast to hyphae differentiation. Furthermore, they suggest that the downregulation of Myo2^{Sj} and Myp2^{Sj} by Rlc1 phosphorylation is independent of the presence of a shorter N-terminus.

A putative alpha-helical motif within the long N-terminus of Rlc1^{Sp} is essential for phosphorylation-dependent regulation of Myo2 function during cytokinesis in *S. pombe*.

In vivo phosphorylation of Rlc1^{Sp} at Ser35 has a minimal effect on myosin II function during CAR dynamics when *S. pombe* cells grow fermentatively on glucose, but it becomes essential for cytokinesis and cell growth during respiratory metabolism [22]. Accordingly, in contrast to *S. pombe rlc1*Δ cells expressing a wild-type and phosphorylated Rlc1^{Sp}-GFP fusion, those expressing a Rlc1^{Sp} (S35A)-GFP mutant version, which is not phosphorylated *in vivo* as confirmed by *Phos tag* SDS-PAGE (Figure 5A), undergo a marked cytokinetic delay and a reduction in the ring constriction rate when transferred to a respiration-based medium containing glycerol (Figure 5B, 5C). This resulted in a progressive increase in multiseptated cells and defective growth in solid medium (Figure 5D, 5E) [22]. Unexpectedly, expression of a wild-type and non-phosphorylated Rlc1^{Sj}–GFP fusion (Figure 5A), allowed a robust cytokinesis and growth of *S. pombe rlc1*Δ cells during respiration (Figure 5B-5E). Cells expressing the phosphorylated Rlc1^{Sj} (N23S)-GFP mutant (Figure 5A) showed a minimal but reproducible cytokinetic delay (Figure 5B) and a small increase in multiseptated cells (Figure 5D). However, these defects did not affect cell proliferation with glycerol (Figure 5E). Secondary structure prediction of Rlc1^{Sp} with RaptorX [39], revealed that the phosphorylated Ser35 in Rlc1^{Sp} lies within a 22 amino-acid putative alpha-helix motif (hereafter α1 helix) of an extended N-terminal sequence that is absent from the N-terminus of Rlc1^{Sj} (Figure S4A). Comparative prediction of three-dimensional structures and superposition analysis with AlphaFold 2.0 [40] also revealed the presence of this motif at the N-terminus of Rlc1^{Sc} and Rlc1^{So}, which is preceded by an unstructured sequence of 20 amino-acids (Figure 5F; Figure S4B). In contrast, the shorter N- terminal tail in Rlc1^{Sj}, including the -KRINS-sequence with the unphosphorylatable Asn23, defines an intrinsically unstructured region (Figure 5A; Figure

S4A). It is possible that the putative α1 helix in Rlc1^{Sp} strongly influences the regulation of myosin II function through phosphorylation at Ser35. Consistent with this hypothesis, expression of an Rlc1^{Sp} version lacking the 15 amino-acids immediately upstream of Ser35 (sequence -NTTSSQRVAAQAAKR-; Rlc1^{Sp} (Δ19-33)-GFP construct) (Figure 5A; Figure S4A), was phosphorylated *in vivo* (-SSASS- motif, hereafter referred to as S20 in Δ19-33 constructs) (Figure 5A) and suppressed the cytokinesis and respiratory growth defects of *rlc1*Δ cells in a similar fashion than the unphosphorylated version Rlc1^{Sp} (Δ19-33, S20A)-GFP (Figure 5A-5E). *In vivo* phosphorylation at Ser20 in the Rlc1^{Sp} (Δ19-33)-GFP allele was also PAK-dependent, as confirmed by the absence of light chain phosphorylation in cells carrying the hypomorphic allele *pak1-M460G* (Figure 5G) [20]. Finally, expression of a chimera with the N-terminal 1 to 25 aa of *S. japonicus* Rlc1 ^{Sj}, including the unphosphorylated Asp23 followed by the *S. pombe* Rlc1^{Sp} amino-acid sequence (Rlc1$^{Sp\ (Nterm\ Sj\ 1\text{-}25)}$-GFP) (Figure 5A; Figure S4A), was also fully functional during *S. pombe* cytokinesis under respiration (Figure 5B-5E). Thus, the precise regulation of myosin II (Myo2) function by phosphorylated Rlc1^{Sp} becomes biologically relevant for *S. pombe* cytokinesis and respiratory growth only in presence of the α1 helix at its N-terminus.

Phosphorylation-induced folding of Rlc1^{Sp} α1 helix into an open conformation allows for critical regulation of cytokinesis by Myo2 ^{Sp} during respiration.

Previous work in animal cells has suggested that phosphorylation of RLC at Ser19 can shift its equilibrium from a closed to an open state, moving the N-terminus further away from the C-terminal lobe to adopt a more helical but flexible conformation [41]. The phosphorylatable Ser35 within the α1 helix in Rlc1^{Sp} is in very close proximity (<5Å) to form hydrogen bonds with Thr104 and Ser108, which are located on the α5 helix. This is not the case for the equivalent α4 helix residues Thr92 and Ser96 with respect to the non-phosphorylatable Asn23 within the unstructured N-terminus of Rlc1^{Sj}, which adopts a more flexible and open structure (Figure 6A). Indeed, modeling and superposition analysis revealed that the α1 helix in the phospho-mimicking mutant Rlc1^{Sp} -S35D, which exhibits normal CAR dynamics and growth during respiration when expressed in *S. pombe* [22], has a more open conformation as compared to the Rlc1^{Sp} (wild-type) and Rlc1^{Sp} -S35A versions (Figure 6B). Thus, this specific and phosphorylation-dependent conformational change in the Rlc1^{Sp} α1 helix may be the critical for the precise regulation of Myo2^{Sp} function during cytokinesis. We found

that substitution of both Thr104 and Ser108 in the Rlc1^{Sp} α5 helix for two bulky tryptophan residues (Rlc1^{Sp}-T104W S108W mutant) predicted to shift the α1 helix towards an open conformation, similar to the phospho-mimic mutation Rlc1^{Sp}-S35D (Figure 6B). The Rlc1^{Sp}-(T104W S108W)-GFP fusion was phosphorylated at Ser35 *in vivo* (Figure 6C) and suppressed the cytokinetic and growth defects of *S. pombe rlc1*Δ cells during respiration in a similar manner to the wild-type Rlc1^{Sp}- GFP (Figure 6D-6G). Strikingly, the introduction of the T104W and S108W mutations in the Rlc1^{Sp}-S35A allele (Rlc1^{Sp}- (S35A T104W S108W)-GFP) (Figure 6B) was sufficient to restore cytokinesis and growth of *rlc1*Δ cells during respiration, despite not being phosphorylated at Ser35 *in vivo* (Figure 6C-6G). Thus, our results confirm that a phosphorylation-dependent mechanism that induces a shift in the Rlc1^{Sp} α1 helix from a closed to an open state is responsible for modulating Myo2^{Sp} activity during cytokinesis. This regulatory mechanism, which is absent in *S. japonicus*, was thus a late acquisition during the evolution of the fission yeast clade.

DISCUSSION

Functional conservation of RLC and myosin II heavy chains during cytokinesis within the fission yeast clade

The two myosin II heavy chains Myo2^{Sj} and Myp2^{Sj} play fundamental and distinct roles during cytokinesis in *S. japonicus*. Myo2^{Sj} is essential for cell viability, localizes to the CAR, and positively regulates the entire cytokinesis process, starting from node assembly and coalescence into a mature ring to the final constriction step. However, Myp2^{Sj} plays a non-essential role and is targeted to the mature CAR to favor ring closure during unperturbed growth and under high osmolarity conditions. Furthermore, RLC Rlc1^{Sj} plays a major role in regulating the function of both heavy chains during cytokinesis, as *rlc1*Δ cells integrate the cytokinetic defects (longer times for ring maturation and constriction, reduced constriction rate and multiseptation), and stress-sensitive phenotypes of Myo2^{Sj} and Myp2^{Sj} mutants. The specific biological roles of Myo2^{Sj}, Myp2^{Sj} and Rlc1^{Sj} as positive modulators of cytokinesis in *S. japonicus* are similar to those early ascribed to their respective orthologs in *S. pombe* [9-12], suggesting that they are evolutionarily conserved within the genus *Schizosaccharomyces*.

Interphase Myo2^{Sj} -Rlc1^{Sj} nodes downregulate S. japonicus yeast to hyphae onset but are required for

full myceliation

Mutants lacking myosin II gene orthologs in pathogenic plant or human filamentous fungi accumulate multiple branched hyphae and abnormal septa, resulting in defective mycelial growth and reduced virulence [4-8]. Myosin II function is also essential for hyphal differentiation and myceliation in *S. japonicus*. However, this control is exerted exclusively by Myo2^{Sj} and Rlc1^{Sj}, whereas Myp2^{Sj} function is dispensable. Most fungal mycelia are multinucleate and lack or contain unconstricted and incomplete septa [42]. In contrast, *S. japonicus* develops a fragmented mycelium composed of mononuclear hyphae that undergo complete septation and division after mitosis and resume a lateral growth pattern behind the recently formed septum [33,43]. Thus, the limited mycelia growth observed in the absence of Myo2^{Sj} and/or Rlc1^{Sj} function is most likely due to the accumulation of multiseptated hyphae that cannot fully separate and undergo further tip extension. Exquisite cytokinetic control of Myo2^{Sj} activity by Rlc1^{Sj} is therefore critical to ensure the unusual mode of hyphal formation and myceliation in this dimorphic fission yeast.

Despite their positive role in mycelial formation, the onset of yeast to hypha differentiation is accelerated in Myo2^{Sj} and Rlc1^{Sj} mutants as compared to the wild type, as revealed by the premature appearance of transition forms. Yeast and hyphal growth in *S. japonicus* relies on vesicle transport on actin cables for polarized growth, which is increased in transition forms and hyphae [33]. Interestingly, we also observed premature hyphal development in the absence of the medial ring protein Mid1, which anchors Myo2^{Sj} and Rlc1^{Sj} nodes to the equatorial cortex during interphase [34]. These nodes, which in *S. pombe* remain cytosolic until early mitosis, are present in *S. japonicus* at the equatorial region in transition forms and hyphae also during the dimorphic switch, and may function by spooling actin cables or participating in vesicular trafficking during polarized growth [44]. However, the actin cable-to-patch ratio and the tip growth rate during hyphal induction were identical between wild type, *rlc1*Δ, *GFP-Myo2* and *mid1*Δ cells. This rule out the possibility that mis-regulated Myo2^{Sj} could induce premature hyphal development by enhancing actin cable and/or vesicle trafficking. Our results strongly suggest that interphase cortical Myo2 ^{Sj}-Rlc1^{Sj} nodes negatively modulate the onset of the yeast-to-hyphae transition in *S. japonicus* by a mechanism that remains to be elucidated.

Evolutionary diversification of regulatory light chain control of myosin II during cytokinesis in fission

yeasts

In animal cells, *in vivo* phosphorylation of RLC at Ser19 is essential for non-muscle myosin II to adopt an extended conformation and assemble into bipolar filaments with increased actin affinity and motor activity [1-3]. Recent resolution of the autohinibited cryoEM structure of NMII [45-47], suggests that N-terminal phosphorylation of RLC at Thr-18 and Ser19 would repeal the negatively charged region of segment 3 of the myosin tail. This, combined with the proposed adoption of an open structural state with a more helical and globally flexible conformation [41], may release the myosin tail and disrupt its shutdown state [45-47].

Instead, *S. pombe* Myo2^{Sp} lacks the propensity to self-assemble *in vitro*, localizes to the plasma membrane in polarized clusters, and is assembled by node binding rather than rod–rod associations [21,48]. N-terminal Rlc1^{Sp} phosphorylation at Ser35 is strongly required to support myosin II activity during cytokinesis when *S. pombe* cells grow by respiratory metabolism, but not during glucose fermentation [22]. Our findings, based on the prediction of three-dimensional structures and the functional characterization of a series of chimeric and point-mutated constructs, strongly suggest that i- *in vivo* phosphorylation of Rlc1^{Sp} at Ser35 by the PAK kinases Pak1/2 induces a shift in its N-terminal α1 helix from a closed to an open state, and ii- this conformational change is essential for the modulation of Myo2^{Sp} activity and cytokinesis under respiratory conditions. Consistent with this model, a shift induced by substitution of the proximal Thr104 and Ser108 of the α5 helix for two tryptophan residues bypassed the requirement for Rlc1^{Sp} phosphorylation at Ser35 to regulate cytokinesis by Myo2^{Sp} during respiration. These observations strongly support the proposed mechanism by which RLC phosphorylation at Ser19 can trigger NMII activation in animal cells [41], which may have been acquired early in the evolution of eukaryotes.

Rlc1^{Sj}, which lacks both the N-terminal α1 helix and the regulatory phosphorylation site, was fully functional to regulate cytokinesis in *S. pombe* during respiration. This unexpected observation may be explained by considering that the unstructured N-terminus of Rlc1^{Sj} constitutively adopts a flexible and open conformation that mimics Rlc1^{Sp} phosphorylation and is therefore able to regulate Myo2^{Sp} activity. Hence, the fission yeast clade represents a remarkable example of evolutionary diversification in the modulation of myosin II activity by the regulatory light chain from a constitutive (*S. japonicus*) to a phosphorylation-dependent “on/off” mechanism (*S. pombe*).

The advantage of Rlc1 control by phosphorylation seems obvious, as it provides an additional layer of

regulation for precise spatio-temporal modulation of myosin II activity. This regulatory mechanism has been adopted across different eukaryotic lineages, including animal cells, where the fine-tuning mechanisms that control NMII function during cell adhesion, migration and division depend on RLC phosphorylation by different kinases at Thr18 and Ser19[1]. So, why is Rlc1^{Sj} fully functional for cytokinesis control in *S. pombe* despite the absence of this this seemingly more restrictive regulatory mechanism? One simple explanation is that early diversification in fission yeast resulted in two different but perfectly matched solutions for Rlc1 regulation of myosin II activity. However, this may be true for *S. pombe* but not for *S. japonicus*, since the phosphorylatable Rlc1^{Sp} version is detrimental to cytokinesis and hyphal differentiation when expressed in this fission yeast species. Alternatively, it is possible that *S. pombe* Rlc1^{Sp} regulates a process other than cytokinesis, which is currently unknown and cannot be sustained by the Rlc1^{Sj} ortholog. Future studies will help to improve our understanding of the relationship between the structure and function of the myosin II light chain in the eukaryotic lineage and its impact on the execution of essential cellular processes.

Limitations of the study

Our results strongly support that Rlc1^{Sj} and Myo2^{Sj} negatively modulate the onset of the yeast to hyphae transition in *S. japonicus*; however, their function is instead essential for full hyphal differentiation and myceliation. Further work will be required to disclose the mechanism/s responsible for the divergent functional roles of myosin II during the dimorphic switch in this organism. Also, our genetic and *in vivo* data are consistent with the structural predictions made by AlphaFold that phosphorylation of Rlc1^{Sp} on residue S35 promotes its shift to an open conformation-state which is essential for Myo2^{Sp} regulation and cytokinesis during respiration. This mechanism does not occur with the unphosphorylatable Rlc1^{Sj}, which adopts a "perpetual" occupation of the open conformation-state. However, if wild-type Rlc1^{Sj} is constitutively in an open conformation state then it is unclear how the addition of a phosphorylation site would alter its function. Thus, additional structural and biophysical work would be needed to provide more insight into the mechanisms behind the phosphorylation-dependent (*S. pombe*) and independent (*S. japonicus*) strategies for RLC regulation of myosin II activity.

ACKNOWLEDGMENTS

We thank Hironori Niki, Snezhana Oliferenko and Pilar Pérez for fission yeast strains and plasmids, and to Pilar Pérez for stimulating discussions and continuous support. This research was funded by Grant PID2020-112569GB-I00 by MCIN/AEI/10.13039/501100011033. F.P.-R. is a Formación de Profesorado Universitario PhD fellow from Ministerio de Educación y Formación Profesional, Spain.

AUTHORS CONTRIBUTIONS

Conceptualization, M.M. and J.C.; Methodology, F.P.-R., E.G.-G., J.V.-S., and A.F.; Investigation, F.P.-R., E.G.-G., J.V.-S., A.F. and T.S.; Writing – Original Draft, J.C..; Writing – Review & Editing, F.P.-R. and M.M.; Funding Acquisition, J.C.; Resources, J.V.-S, M.M., and J.C..; Supervision, M.M and J.C.

DECLARATION OF INTERESTS

The authors declare no competing interests.

FIGURE LEGENDS

Figure 1. Rlc1^{Sj} is a positive regulator of cytokinesis in *S. japonicus*.

(A) ClustalW analysis (https://www.ebi.ac.uk/Tools/msa/clustalo/) of the amino acid sequences of the regulatory light chain Rlc1 in the fission yeast species *S. pombe*, *S. octosporus*, *S. cryophilus* and *S. japonicus*. The extended N-terminal motif, present in all fission yeast species except *S. japonicus*, is shown within a square with a dotted line. Black arrow: Pak1/Pak2-dependent Ser35 phosphorylation site in Rlc ^{Sp}. *: The corresponding position in Rlc1^{Sj} is changed to an asparagine residue.

(B) Representative maximum-projection time-lapse images of Rlc1-mCherry dynamics at the equatorial region of *S. japonicus* cells growing in YES-glucose. Mitotic progression was monitored using Pcp1-mCherry-labeled SPBs. Time interval is 4 min. Scale bar: 10 µm.

(C) Upper: Strains of the indicated genotypes were grown in YES-glucose medium through the exponential and stationary phases of growth, incubated at 37ºC or treated with 1M KCl for 12 h, and the percentage of septated and multiseptated cells was quantified. Data correspond to three independent experiments and are presented as mean ± SD. Statistical comparison between wild type and *rlc1Δ* cells was performed by unpaired

Student's t-test. ****, p<0.0001; ***, p<0.0005; **, p<0.005; *, p<0.05; ns, not significant. Lower: representative maximum projection confocal images of cells from the indicated strains grown for 24h on YES-glucose after cell-wall staining with calcofluor white. Arrows indicate incomplete septa/multiseptated cells. Scale bar: 10 µm.

(D) Decimal dilutions of strains of the indicated genotypes were spotted on plates with YES or YES plus 1.2 M K Cl, incubated at 28°C or 42ºC for 3 days, and photographed. Images correspond to representative experiments that were repeated at least three times with similar results.

(E) Left: Times for node condensation/ring maturation, ring constriction and disassembly, and ring assembly and contraction were estimated by time-lapse confocal fluorescence microscopy for the indicated strains expressing a genomic Cdc15-GFP fusion and growing exponentially in YES-glucose medium. Mitotic progression was monitored using Pcp1-mCherry-labeled SPBs. Right: Ring constriction rates (µm/min), were determined for the indicated strains. n is the total number of cells scored from three independent experiments, and data are presented as violin plots. Statistical comparison between two groups was performed by unpaired Student's t-test. ***, p<0.0005.

(F) Representative maximum-projection time-lapse images of Cdc15 dynamics at the equatorial region of cells growing in YES-glucose. Mitotic progression was monitored using Pcp1-mCherry-labeled SPBs. Time interval is 4 min. Scale bar: 10 µm.

Figure 2. Rlc1^{Sj} negatively regulates the onset of yeast to hypha differentiation in *S. japonicus* but is required for myceliation.

(A) Left: Representative DIC images of wild-type and *rlc1*Δ cells incubated in RGE-agarose pads at 30 ºC for the indicated times. Arrows: transition forms. Asterisks: hyphae. Scale bar: 10 µm. Middle: Percentages of transition forms and hyphae were determined for the indicated times in cells incubated in RGE-agarose pads. Data correspond to three independent experiments and are presented as mean ± SD. Right: Transition form elongation rates (µm/min) were determined for the indicated strains. n is the total number of cells evaluated

from three independent experiments, and data are presented as scatter plots. Statistical comparison between two groups was performed by unpaired Student's t-test. ns, not significant.

(B) The percentages of yeasts, transition forms and hyphae were determined in wild-type and *rlc1*Δ strains after incubation for the indicated times in YES-glucose medium supplemented with 0.2 µM CPT. Data correspond to three independent experiments and are presented as mean ± SD.

(C) Left: cells from log-phase cultures of the indicated strains growing in YES medium (~2.10^6 cells in each case) were spotted on YEMA and RGE plates, incubated at 30°C for 7 days, and then photographed. Right: Total area of mycelial expansion (expressed in relative units, RU) was measured for each strain genotype (n=5) and shown as a scatter plot. ****, P<0.0001, as calculated by unpaired Student's t-test.

(D) Cells from log-phase cultures of wild-type and *rlc1*Δ strains were spotted on semi-solid RGE-gelatin plates and incubated at 30°C for 10 days. Hyphae were collected, stained with calcofluor white, and photographed. Scale bar: 10 µm.

(E) Left: Lengths of wild-type and *rlc1*Δ hyphae recovered in **(D)** were measured. n is the total number of hyphae scored from three independent experiments, and data are presented as scatter plots. Statistical comparison between two groups was performed by unpaired Student's t-test. ****, P<0.0001. Right: The percentage of multiseptated hyphae was quantified. Data correspond to three independent experiments and are presented as mean ± SD. ****, P<0.0001, as calculated by unpaired Student's t-test.

Figure 3. Rlc1^{Sj} regulates Myo2^{Sj} and Myp2^{Sj} during cytokinesis, whereas Rlc1^{Sj}-Myo2^{Sj} modulate yeast to hyphae onset and mycelium development.

(A) Representative maximum-projection time-lapse images of Myp2 and Rlc1 dynamics at the CAR in cells co-expressing Myp2-GFP and Rlc1-mCherry genomic fusions and grown in YES-glucose. Mitotic progression was monitored using Pcp1-mCherry-labeled SPBs. Scale bar: 10 µm.

(B) Decimal dilutions of strains of the indicated genotypes were spotted on plates with YES or YES plus 1.2 M K Cl, incubated at 28°C or 42ºC for 3 days, and photographed. The images correspond to representative experiments that were repeated at least three times with similar results.

(C) Strains of the indicated genotypes were grown in YES-glucose medium and incubated at 30º, 37ºC, or treated with 1M KCl for 12 h, and the percentage of septated and multiseptated cells was quantified. Data

correspond to three independent experiments and are presented as mean ± SD. Statistical comparison was performed by one-way ANOVA. ****, p<0.0001; ***, p<0.0005**;** **, p<0.005**;** ns, not significant.

(D) Left: Times for node condensation/ring maturation, ring constriction and disassembly, and ring assembly and contraction were estimated by time-lapse confocal fluorescence microscopy for GFP-Myp2 cells, and wild type and *rlc1*Δ cells expressing a genomic Rlc1-GFP fusion and growing exponentially in YES-glucose medium. Mitotic progression was monitored using Pcp1-mCherry-labeled SPBs. Right: Ring constriction rates (μm/min), were determined for the indicated strains. n is the total number of cells scored from three independent experiments, and data are presented as violin plots. Statistical comparison between two groups was performed by one-way ANOVA. ****, p<0.0001; ns, not significant.

(E) Representative maximum-projection time-lapse images of Rlc1-GFP and GFP-Myo2 dynamics at the equatorial region of cells growing in YES-glucose. Mitotic progression was monitored using Pcp1-mCherry-labeled SPBs. Scale bar: 10 μm.

(F) The percentages of transition forms and hyphae were determined for the indicated strains incubated in RGE-agarose pads. Data correspond to three independent experiments and are presented as mean ± SD.

(G) Cells from log-phase cultures of the indicated strains growing in YES medium were spotted on YEMA and RGE plates, incubated at 30°C for 7 days, and then photographed.

(H) The total area of mycelial expansion (expressed in relative units, RU) was measured for each strain genotype (n≥3) and shown as a scatter plot. ****, P<0.0001; ns, not significant, as calculated by one-way ANOVA.

Figure 4. *In vivo* phosphorylation of Rlc1 is detrimental for Myo2 function during *S. japonicus* cytokinesis hyphal differentiation.

(A) Total protein extracts from the indicated *S. japonicus* strains expressing the indicated $Rlc1^{Sp}$- and $Rlc1^{Sj}$-GFP constructs grown exponentially in YES-glucose medium were resolved by Phos-tag SDS-PAGE, and the Rlc1-GFP fusion was detected by incubation with anti-GFP antibody. Anti-Cdc2 was used as a loading control. Phosphorylated Rlc1 isoforms are indicated by an asterisk (*). The blot corresponds to a representative experiment that was repeated at least three times and the trend of the mobility shift was reproducible.

(B) Decimal dilutions of strains of the indicated genotypes were spotted on plates with YES or YES plus 1.2 M K Cl, incubated at 30°C or 40ºC for 3 days, and photographed. Images correspond to representative experiments that were repeated at least three times with similar results.

(C) Upper: Times for node condensation/ring maturation, ring constriction and disassembly, and ring assembly and contraction were estimated by time-lapse confocal fluorescence microscopy for the indicated strains expressing different Rlc1^{Sp}- and Rlc1^{Sj}- GFP fusions and growing exponentially in YES-glucose medium. Mitotic progression was monitored using Pcp1-mCherry-labeled SPBs. Lower: Ring constriction rates (μm/min), were determined for the indicated strains. n is the total number of cells scored from three independent experiments, and data are presented as violin plots. Statistical comparison between two groups was performed by one-way ANOVA. ****, p<0.0001; *, p<0.05; ns, not significant.

(D) Representative maximum-projection time-lapse images of Rlc1-GFP dynamics at the equatorial region of cells of the indicated strains growing in YES-glucose. Mitotic progression was monitored using Pcp1-GFP-labeled SPBs. Scale bar: 10 μm.

(E) The percentages of transition forms and hyphae were determined for the indicated strains incubated in RGE-agarose pads. Data correspond to three independent experiments and are presented as mean ± SD.

(F) Cells from log-phase cultures of the indicated strains growing in YES medium were spotted on YEMA and RGE plates, incubated at 30°C for 7 days, and then photographed.

(G) The total area of mycelial expansion (expressed as relative units, RU) was measured for each strain genotype (n≥6) and shown as a scatter plot. ****, P<0.0001; ns, not significant, as calculated by one-way ANOVA.

Figure 5. N-terminal α1 helix in Rlc1^{Sp} is critical for phosphorylation-dependent modulation of Myo2^{Sp} activity in *S. pombe* during cytokinesis.

(A) Total protein extracts from the indicated *S. pombe* strains expressing the indicated Rlc1^{Sp}-GFP and Rlc1^{Sj}-GFP constructs grown exponentially in YES-glucose medium were resolved by Phos-tag SDS-PAGE, and the Rlc1-GFP fusion was detected by incubation with anti-GFP antibody. Anti-Cdc2 was used as a loading control. Phosphorylated Rlc1 isoforms are indicated with an asterisk (*). The blot corresponds to a

representative experiment that was repeated at least three times and the trend of the mobility shift was reproducible.

(B) Left: Times for node condensation/ring maturation, ring constriction and disassembly, and ring assembly and contraction were estimated by time-lapse confocal fluorescence microscopy for the indicated *S. pombe* strains expressing different $Rlc1^{Sp}$- and $Rlc1^{Sj}$- GFP fusions and growing exponentially in YES-glycerol medium. Mitotic progression was monitored using Pcp1-mCherry-labeled SPBs. Right: Ring constriction rates (μm/min), were determined for the indicated strains. n is the total number of cells scored from three independent experiments, and data are presented as violin plots. Statistical comparison between two groups was performed by one-way ANOVA. ****, $p<0.0001$; **, $p<0.005$; ns, not significant.

(C) Representative maximum-projection time-lapse images of $Rlc1^{Sp}$-GFP and $Rlc1^{Sj}$- GFP dynamics at the equatorial region of cells of the indicated *S. pombe* strains growing in YES-glycerol. Mitotic progression was monitored using Pcp1-GFP-labeled SPBs. Scale bar: 10 μm.

(D) *S. pombe* strains expressing the indicated $Rlc1^{Sp}$-GFP and $Rlc1^{Sj}$- GFP constructs growing exponentially in YES-glucose were harvested and incubated in YES-glycerol medium for 16 h, and the percentage of septated and multiseptated cells was quantified. Data correspond to three independent experiments and are presented as mean ± SD. Statistical comparison was performed by one-way ANOVA. Statistical comparison was performed by one-way ANOVA. ****, $p<0.0001$; *, $p<0.05$**;** ns, not significant.

(E) Decimal dilutions of strains of the indicated genotypes were spotted onto plates with YES-glucose or YES-glycerol plates, incubated at 28°C for 3 (Glc) or 5 (Gly) days, and photographed. The images correspond to a representative experiment, which was repeated at least three times with similar results.

(F) AlphaFold2 prediction of $Rlc1^{Sp}$ and $Rlc1^{Sj}$ wild type and mutant versions. The position of the phosphorylatable Ser35 in $Rlc1^{Sp}$ is indicated by an arrow. Superposition of $Rlc1^{Sp}$ (grey) and $Rlc1^{Sj}$ (orange) 3D models was performed using PyMOL 2.5 (https://pymol.org/2/).

(G) Total protein extracts from *S. pombe* wild type and *pak1-M460G* strains expressing the indicated $Rlc1^{Sp}$-GFP and $Rlc1^{Sj}$- GFP constructs grown exponentially in YES-glucose medium were resolved by Phos-tag SDS-PAGE, and the Rlc1-GFP fusion was detected by incubation with anti-GFP antibody. Anti-Cdc2 was used as a loading control. Phosphorylated Rlc1 isoforms are indicated by an asterisk (*). The blot corresponds

to a representative experiment that was repeated at least three times and the trend of the mobility shift was reproducible.

Figure 6. Phosphorylation-induced folding of Rlc1^{Sp} α1 helix into an open conformation allows precise Myo2^{Sp} regulation during cytokinesis and respiration.

(A) Boxed regions in the AlphaFold2 predictions are shown enlarged to highlight the differences in the N-terminal extensions between Rlc1^{Sp} and Rlc1^{Sj}. The positions of the phosphorylatable Ser35 in the Rlc1^{Sp} α1 helix and the non-phosphorylatable Asn23 in the unstructured Rlc1^{Sp} N-terminus are indicated. Side chains of the nearby residues Thr104 and Ser108 located on the proximal α5 helix in Rlc1^{Sp} (Thr92 and Ser96 in Rlc1^{Sj}) are also shown.

(B) Overlay of Rlc1^{Sp} (dark blue) vs Rlc1^{Sp} (S35A) (green), Rlc1^{Sp} (S35D) (grey), Rlc1^{Sp} (T104W S108W) (orange) and Rlc1^{Sj} (S35A T104W S108W) (magenta) and Rlc1^{Sp} (S35A) (green) vs Rlc1^{Sj} (S35A T104W S108W) (magenta) 3D models were performed using PyMOL 2.5 (https://pymol.org/2/).

(C) Total protein extracts from *S. pombe* strains expressing the indicated Rlc1^{Sp}-GFP constructs grown exponentially in YES-glucose medium were resolved by Phos-tag SDS-PAGE, and the Rlc1-GFP fusion was detected by incubation with anti-GFP antibody. Anti-Cdc2 was used as a loading control. Phosphorylated Rlc1 isoforms are indicated with an asterisk (*). The blot corresponds to a representative experiment that was repeated at least three times and the trend of the mobility shift was reproducible.

(D) Upper: Times for ring assembly and contraction, node condensation/ring maturation and ring constriction and disassembly were estimated by time-lapse confocal fluorescence microscopy for the indicated *S. pombe* strains expressing different Rlc1^{Sp}- GFP fusions and growing exponentially in YES-glycerol medium. Mitotic progression was monitored using Pcp1-mCherry-labeled SPBs. Lower: Ring constriction rates (μm/min), were determined for the indicated strains. n is the total number of cells scored from three independent experiments, and data are presented as violin plots. Statistical comparison between two groups was performed by one-way ANOVA. ****, $p<0.0001$; **, $p<0.005$; ns, not significant.

(E) Representative maximum-projection time-lapse images of Rlc1^{Sp}-GFP dynamics at the equatorial region of cells of the indicated *S. pombe* strains growing in YES-glycerol. Mitotic progression was monitored using Pcp1-GFP-labeled SPBs. Scale bar: 10 μm.

(F) *S. pombe* strains expressing the indicated Rlc1^{Sp}-GFP constructs growing exponentially in YES-glucose were recovered and incubated in YES-glycerol medium for 16 h, and the percentage of septated and multiseptated cells was quantified. Data correspond to three independent experiments and are presented as mean ± SD. Statistical comparison was performed by one-way ANOVA. Statistical comparison was performed by one-way ANOVA. ****, $p<0.0001$; ***, $p<0.0005$; *, $p<0.05$**;** ns, not significant.

(G) Decimal dilutions of strains of the indicated genotypes were spotted onto plates with YES-glucose or YES-glycerol plates, incubated at 28°C for 3 (Glc) or 5 (Gly) days, and photographed. The images correspond to a representative experiment, which was repeated at least three times with similar results.

STAR METHODS

RESOURCE AVAILABILITY

Lead contact

Further information and requests for resources, strains and reagents should be directed to and will be fulfilled by the lead contact, Jose Cansado (jcansado@um.es).

Materials availability

Plasmids and strains generated are available upon request to the lead contact.

Data and code availability

• This paper does not report original code

• Source data corresponding to the main and supplemental figures have been deposited at Mendeley and are publicly available as of the date of publication. The DOI is listed in the key resources table.

• Any additional information required to reanalyze the data reported in this work paper is available from the lead contact upon request.

Experimental Model and Study Participant Details

The genotypes of *S. pombe* and *S. japonicus* fission yeast strains used in this study are shown in Table S1.

Method Details

Fission yeast strains and growth conditions

S. pombe and S. *japonicus* strains were grown routinely with shaking at 28ºC in YES-glucose medium containing 0.6% yeast extract, 2% glucose and supplemented with adenine, leucine, histidine, or uracil (100 mg/liter)[49]. Mutant strains with single or multiple gene deletions or expressing genomic fusions were obtained by transformation, or after tetrad/ random spore dissection and analysis of appropriate crosses in sporulation medium (SPA) [50].Transformation of *S. japonicus* by electroporation was performed following the protocol described in [51]. Briefly, early log phase cells growing in YES medium at 30°C were recovered by filtration, washed in sterile water, and incubated for 15 min at 30°C with 1 M sorbitol plus 50 mM DTT. The

cells were then resuspended in 1M sorbitol, 0.5 to 1 µg DNA was added, and the DNA-cell mixture was placed into a prechilled (4°C) 0.2-cm cuvette and electroporated under the following conditions: 2.3 kV, 200 Ω, and 25 µF. The cell mixture was recovered from the cuvette into 10 ml of YE medium and leave overnight at 30°C. Finally, aliquots of the electroporated cells were plated on appropriate selection agar plates and incubated for 2–3 days. For stress treatments, log-phase cultures (OD_{600}= 0.5; ~10^6 cells/ml) were supplemented with 1M KCl (osmotic-saline stress; Sigma-Aldrich) or incubated at 37ºC (thermal stress). For *time-lapse* imaging of CAR dynamics, overnight cultures in YES-glucose were diluted to an OD_{600} of 0.01 and incubated until reaching a final OD_{600} of 0.2. Then, cells were recovered by filtration, washed three times, and transferred to either YES-glucose or YES-glycerol (0.6% yeast extract, 0.08% glucose, 0.86% glycerol, plus supplements) and incubated at 28ºC for 4 h before imaging. For yeast to hyphae induction experiments with *S. japonicus*, log-phase cultures grown in YES medium with 6% glucose were treated with camptothecin (CPT; Sigma-Aldrich) to a final concentration of 0.2 µM. YEMA [30] and RGE [33] media supplemented with 2% agarose or 10% gelatin [37] were used to quantify *S. japonicus* mycelial growth.

S. japonicus gene disruption and gene fusion

Sequences of *S. japonicus* genes were obtained from the annotated database at *EnsemblFungi* (http://fungi.ensembl.org/Schizosaccharomyces_japonicus/Info/Index?db=core). Null mutants in the *rlc1*$^+$ and *myp2*$^+$ genes were obtained by ORF deletion and replacement with the nourseothricin (NAT) cassette by a PCR-mediated strategy using plasmid pFA6a-*natMX6* [52,53]. The plasmid pFA6a-GFP-*natMX6* was used to obtain a genomic C-terminal Myp2-GFP-tagged version. *Nat*^{R} transformants were obtained, and the correct gene-deletion and expression of the fusion were verified by both PCR and/or Western blot analysis. Oligonucleotides employed in each case are shown in Table S2.

Construction of *S. pombe* and *S. japonicus* strains expressing wild type and chimeric Rlc1-GFP fusions

Constructs expressed in *S. japonicus*.

The integrative plasmids pSL-Rlc1^{Sj}-GFP and pSL-Rlc1^{Sp}-GFP were obtained in three consecutive steps. First, the *rlc1*$^{+Sj}$ endogenous promoter was amplified by PCR using genomic DNA from the wild-type strain *S. japonicus* 2017h$^+$ as template and the 5' and 3' oligonucleotides PromRlc1Sj-FWD and PromRlc1Sj/Sj-

REV or PromRlc1Sj/Sp-REV (Supplementary Table S2). Next, Rlc1^{Sj}-GFP and Rlc1^{Sp}-GFP fusions were amplified by PCR using genomic DNA from *S. japonicus* and *S. pombe* strains expressing the respective genomic Rlc1^{Sj}-GFP and Rlc1^{Sp}-GFP fusions as template, and the 5' and 3' oligonucleotides Rlc1Sj-GFP-FWD or Rlc1Sp-GFP-FWD and Rlc1-GFP-REV, respectively. Finally, both fragments were then assembled by Gibson cloning into pSL plasmid linearized with *Sma*I. The resulting plasmids were digested with *Stu*I and transformed into a *rlc1Δ^{Sj} ura4.D3* strain. To introduce the mutations Asn23 to serine (Rlc1^{Sj} ORF) and Ser35 to alanine (Rlc1^{Sp} ORF), the respective pSL-Rlc1$^{Sj/Sp}$-GFP plasmids were subjected to site-directed mutagenesis by PCR using the mutagenic oligonucleotides described in Supplementary Table S2.

Constructs expressed in *S. pombe*.

The integrative plasmids pJK210-Rlc1^{Sj}-GFP and pJK210-Rlc1^{Sp}-GFP were obtained using a strategy like that described above. First, the *rlc1^{+Sp}* endogenous promoter was amplified by PCR using genomic DNA from the wild-type strain *S. pombe* 972h^{-} as template and the 5' and 3' oligonucleotides PromRlc1Sp-FWD and PromRlc1Sp/Sp-REV or PromRlc1Sp/Sj (Supplementary Table S2). Next, Rlc1^{Sj}-GFP and Rlc1^{Sp}-GFP fusions were amplified by PCR using genomic DNA from *S. japonicus* and *S. pombe* strains expressing the respective genomic Rlc1^{Sj}-GFP and Rlc1^{Sp}-GFP fusions as templates, and the respective 5' and 3' oligonucleotides Rlc1Sp/Sj-GFP-FWD or Rlc1Sp/Sp-GFP-FWD and Rlc1-GFP-PJK210-REV. Both fragments were assembled by Gibson cloning into pJK210 plasmid linearized with *Sma*I, and the resulting plasmid was digested with *Bmgb*I and transformed into a *rlc1Δ^{Sp} ura4.194* strain. To introduce the mutations Asn23 to serine (Rlc1^{Sj} ORF), Ser35 to alanine, and Thr104 and Thr108 to triptophan (Rlc1^{Sp} ORF) pJK210-Rlc1$^{Sj/Sp}$-GFP plasmids were subjected to site-directed mutagenesis by PCR. using the mutagenic oligonucleotides described in Supplementary Table S2.

To obtain the integrative plasmids pJK210-Rlc1*Δ19-33*-GFP and pJK210-Rlc1*Δ19-33 S20A*-GFP, the *rlc1^{+Sp}* promoter plus the ORF to residue 19 were amplified by PCR using plasmids pJK210-Rlc1Sp-GFP or pJK210-Rlc1(S35A)Sp-GFP as templates and the 5' and 3' oligonucleotides PromRlc1SpHelix-FWD and PromRlc1SpHelix-REV. The Rlc1Sp-GFP fusion starting from the alanine residue at position 33 was amplified by PCR using the plasmids pJK210-Rlc1Sp-GFP or pJK210-Rlc1(S35A)Sp-GFP as templates and

651 the 5' and 3' oligonucleotides Rlc1SpHelix-FWD and Rlc1-GFP-PJK210-REV. DNA fragments were purified
652 and assembled by Gibson cloning into pJK210 plasmid linearized with *Sma*I. To obtain the integrative
653 plasmid pJK210-Rlc1NtermSj-GFP, the *rlc1*$^{+Sp}$ promoter followed by the corresponding ORF up to the
654 asparagine residue at position 23 was amplified by PCR using DNA from pJK210-Rlc1Sj-GFP as template
655 and 5' and 3' oligonucleotides PromRlc1Sp-FWD and PromRlc1SjNterm-REV. Next, the Rlc1^{Sp} ORF starting
656 at the Serine 36 residue was amplified by PCR using pJK210-Rlc1(S35A)Sp-GFP plasmid as template and 5'
657 and 3' oligonucleotides Rlc1S35A-GFP-FWD and Rlc1-GFP-PJK210-REV. Purified DNA fragments were
658 integrated by Gibson cloning into the *Sma*I linearized pJK210 plasmid. In all cases, the resulting integrative
659 plasmids were digested with *Bmgb*I and transformed into a *rlc1Δ*^{Sp} *ura4.294* strain.
660
661 **Western blot analysis**
662 To determine the levels of Rlc1-GFP fusion and its phosphorylation status in *S. pombe* and *S. japonicus*, 10 ml
663 samples of fission yeast cultures were collected and precipitated with TCA [55]. Protein extracts were resolved
664 on 12% SDS-PAGE gels containing 30μM Phos-tag™ acrylamide (Wako, AAL-107), transferred to
665 nitrocellulose blotting membranes, and immunoblotted with a mouse monoclonal anti-GFP antibody (Roche,
666 11 814 460 001, RRID:AB_390913). Rabbit monoclonal anti-PSTAIR (anti-Cdc2; Sigma-Aldrich, 06-923,
667 RRID:AB_310302) was used as a loading control. Immunoreactive bands were detected using anti-mouse
668 (Abcam, ab205719, RRID:AB_2755049), and anti-rabbit HRP-conjugated secondary antibodies (Abcam,
669 ab205718, RRID:AB_2819160), and the ECL system (GE-Healthcare, RPN2106).
670
671 **Plate assay of stress sensitivity for growth**
672 For the plate assays of growth stress sensitivity, *S. pombe* and *S. japonicus* wild-type and mutant strains were
673 grown in YES-glucose liquid medium to an OD_{600} of 1.2, recovered by centrifugation, resuspended in YES to
674 a density of 10^7 cells/ml, and appropriate decimal dilutions were spotted on YES-glucose supplemented with
675 different concentrations of KCl (Sigma-Aldrich), or YES-glycerol solid plates (2% agar). The plates were
676 incubated for 3 days (YES-glucose) or 5 days (YES-glycerol) at different temperatures (28ºC, 37ºC and/or
677 42ºC), depending on the experiment. All the assays were repeated at least three times with similar results.
678 Representative experiments are shown in the corresponding figures.

679

680 **Quantification of mycelial growth**

681 Approximately 2.10^6 cells from log-phase cultures (OD_{600}= 0.5) of wild type and mutant strains growing in
682 YES-glucose medium were spotted onto YEMA or RGE plates, incubated at 30°C for 7 days, and then
683 photographed and saved as 16-bit .jpg digital images. The area of mycelial expansion was outlined for each
684 strain ($n \geq 6$) by freehand, and measured with ImageJ using the *analyze tool* [56].

685

686 **Microscopy**

687 For *time-lapse* imaging of CAR dynamics in *S. pombe*, 300 µl of cells grown exponentially for 4 h in
688 YES-glucose or YES-glycerol liquid medium, were added to a well of a µ-Slide eight-well chamber (Ibidi,
689 80826) previously coated with 10 µl of 1 mg/ml soybean lectin (Sigma-Aldrich, L2650) [57]. Cells were allowed
690 to sediment and adhere to the bottom of the well for 1 min, and images were taken every 2 or 2.5 min for 2 h
691 (YES-glucose) or every 5 min for 8 h (YES-glycerol). Imaging of CAR dynamics in *S. japonicus* was
692 performed with *50* µl of cells grown exponentially in YES medium applied on YES-agarose pads. Single mid
693 planes were taken from a set of six (*S. pombe*) or nine (*S. japonicus*) 0.61 µm stacks at the indicated time
694 points. Time-lapse images were acquired using a Leica Stellaris 8 confocal microscope with a 63X/1.40 Plan
695 Apo objective controlled by the LAS X software. The time for node condensation and ring maturation
696 includes the time from SPB separation to the onset of CR constriction. Ring constriction and disassembly time
697 includes the time from the first frame of ring constriction to the last frame where the ring is completely
698 constricted and disassembled. The total time for ring assembly and contraction is the sum of these two values.
699 *n* is the total number of cells scored from at least three independent experiments. Ring constriction rates were
700 manually measured as the average circumference ± SD of wild-type and mutant Rlc1-GFP, Rlc1-mCherry or
701 $Cdc15^{Sj}$-GFP versions at contractile rings in each time frame starting from the first frame of CAR constriction.
702 Actin staining of fixed cells with Alexa-Fluor phalloidin was performed following the protocol
703 described in [57]. Briefly, mid-log cultures in YES (5 ml) were fixed for 40 min at 28°C with 1/10 vol of PEM
704 (0.1 M Na PIPES pH 6.8, 1 mM EGTA, 1 mM MgCl2), and 1/5 vol of 16% EM-grade formaldehyde. Cells
705 were then washed three times with 0.5 ml PEM, permeabilized for 30 s with PEM/1% Triton X-100, washed
706 three additional times with PEM, and the cell pellets were resuspended in the remaining liquid. For staining, 8

µl of Alexa fluor 488-conjugated phalloidin (Thermo Fisher Scientific) dissolved in PEM (~6.6 µM) were added to 1 µl of the resuspended cell pellets, and incubated in the dark for 1 hr at room temperature in a rocking platform.Images of stained cells were captured from samples spotted on glass slides using a Leica Stellaris 8 confocal microscope with a 63X/1.40 Plan Apo objective (10 stacks of 0.3 µm each). For actin segmentation analysis, the Ilastik routine was trained with representative images using the pixel classification tool [36] by drawing cables, patches and background in three different colours. Once the program was trained, the remaining images from the different experiments were uploaded to Ilastik to run the segmentation routine. The resulting images were then exported to ImageJ [56] and the segmented cells were analysed using the colour histogram tool to obtain the specific areas corresponding to cables and patches. Data from $n \geq 40$ growing cells were obtained for each cell by dividing the cable area by the patch area, and the ratio was normalized with respect to the average obtained from wild-type cells.

For cell wall staining, cells were recovered from 1 ml aliquots by centrifugation, stained with 1 µl of 0.5 mg/ml calcofluor white, and images were captured from samples spotted on glass slides using a Leica Stellaris 8 confocal microscope with a 63X/1.40 Plan Apo objective (9 stacks of 0.61 µm each). The percentage of septated (one septa) and multiseptated (two or more septa) cells was calculated at the indicated time points for each strain and condition from three independent experiments. $n \geq 100$ cells were counted from multiple images taken during each replicate.

To quantify the increase in cell length during hyphal induction experiments with CPT, samples were taken at the indicated times and immediately fixed with formaldehyde [58]. After staining with calcofluor white, the length of late G2 mononuclear yeast cells, transition forms and hyphae was measured. Three biological replicates ($n \geq 400$) were evaluated for each strain genotype.

QUANTIFICATION AND STATISTICAL ANALYSIS

Statistical analysis was performed using prism 9.0.2. software (Graph Pad), and results are presented as violin plots or mean ± SD, unless otherwise stated. Comparisons between two groups were calculated using unpaired two-tailed Student's t-tests, whereas comparisons between more than two groups were calculated using one-way ANOVA with Bonferroni's multiple comparison test. We observed a normal distribution and no

difference in variance between groups in individual comparisons. Statistical significance: * $p<0.05$; ** $p < 0.005$; *** $p < 0.0005$; **** $p < 0.0001$. Further details of statistical analysis are given in the figure legends.

References

1. Garrido-Casado, M., Asensio-Juárez, G., and Vicente-Manzanares, M. (2021). Nonmuscle Myosin II Regulation Directs Its Multiple Roles in Cell Migration and Division. Annu Rev Cell Dev Biol *37*, 285-310. 10.1146/annurev-cellbio-042721-105528.
2. Craig, R., Smith, R., and Kendrick-Jones, J. (1983). Light-chain phosphorylation controls the conformation of vertebrate non-muscle and smooth muscle myosin molecules. Nature *302*, 436-439. 10.1038/302436a0.
3. Trybus, K.M., and Lowey, S. (1984). Conformational states of smooth muscle myosin. Effects of light chain phosphorylation and ionic strength. J Biol Chem *259*, 8564-8571.
4. Guo, M., Tan, L., Nie, X., and Zhang, Z. (2017). A class-II myosin is required for growth, conidiation, cell wall integrity and pathogenicity of Magnaporthe oryzae. Virulence *8*, 1335-1354. 10.1080/21505594.2017.1323156.
5. Song, B., Li, H.P., Zhang, J.B., Wang, J.H., Gong, A.D., Song, X.S., Chen, T., and Liao, Y.C. (2013). Type II myosin gene in Fusarium graminearum is required for septation, development, mycotoxin biosynthesis and pathogenicity. Fungal Genet Biol *54*, 60-70. 10.1016/j.fgb.2013.02.010.
6. Renshaw, H., Vargas-Muñiz, J.M., Richards, A.D., Asfaw, Y.G., Juvvadi, P.R., and Steinbach, W.J. (2016). Distinct Roles of Myosins in Aspergillus fumigatus Hyphal Growth and Pathogenesis. Infect Immun *84*, 1556-1564. 10.1128/iai.01190-15.
7. Taheri-Talesh, N., Xiong, Y., and Oakley, B.R. (2012). The functions of myosin II and myosin V homologs in tip growth and septation in Aspergillus nidulans. PLoS One *7*, e31218. 10.1371/journal.pone.0031218.
8. Cánovas, D., Boyce, K.J., and Andrianopoulos, A. (2011). The fungal type II myosin in Penicillium marneffei, MyoB, is essential for chitin deposition at nascent septation sites but not actin localization. Eukaryot Cell *10*, 302-312. 10.1128/ec.00201-10.
9. Pollard, T.D., and Wu, J.Q. (2010). Understanding cytokinesis: lessons from fission yeast. In Nat Rev Mol Cell Biol, pp. 149-155. 10.1038/nrm2834.
10. Rincon, S.A., and Paoletti, A. (2016). Molecular control of fission yeast cytokinesis. Semin Cell Dev Biol *53*, 28-38. 10.1016/j.semcdb.2016.01.007.
11. Balasubramanian, M.K., Bi, E., and Glotzer, M. (2004). Comparative analysis of cytokinesis in budding yeast, fission yeast and animal cells. Curr Biol *14*, R806-818. 10.1016/j.cub.2004.09.022.
12. Wang, K., Okada, H., and Bi, E. (2020). Comparative Analysis of the Roles of Non-muscle Myosin-IIs in Cytokinesis in Budding Yeast, Fission Yeast, and Mammalian Cells. Front Cell Dev Biol *8*, 593400. 10.3389/fcell.2020.593400.
13. Gu, Y., and Oliferenko, S. (2015). Comparative biology of cell division in the fission yeast clade. Curr Opin Microbiol *28*, 18-25. 10.1016/j.mib.2015.07.011.
14. Laplante, C., Berro, J., Karatekin, E., Hernandez-Leyva, A., Lee, R., and Pollard, T.D. (2015). Three myosins contribute uniquely to the assembly and constriction of the fission yeast cytokinetic contractile ring. Curr Biol *25*, 1955-1965. 10.1016/j.cub.2015.06.018.
15. Palani, S., Chew, T.G., Ramanujam, S., Kamnev, A., Harne, S., Chapa, Y.L.B., Hogg, R., Sevugan, M., Mishra, M., Gayathri, P., and Balasubramanian, M.K. (2017). Motor Activity Dependent and Independent Functions of Myosin II Contribute to Actomyosin Ring Assembly and Contraction in Schizosaccharomyces pombe. Curr Biol *27*, 751-757. 10.1016/j.cub.2017.01.028.
16. Okada, H., Wloka, C., Wu, J.Q., and Bi, E. (2019). Distinct Roles of Myosin-II Isoforms in Cytokinesis under Normal and Stressed Conditions. iScience *14*, 69-87. 10.1016/j.isci.2019.03.014.
17. Le Goff, X., Motegi, F., Salimova, E., Mabuchi, I., and Simanis, V. (2000). The S. pombe rlc1 gene encodes a putative myosin regulatory light chain that binds the type II myosins myo3p and myo2p. J Cell Sci *113 Pt 23*, 4157-4163.
18. Naqvi, N.I., Wong, K.C., Tang, X., and Balasubramanian, M.K. (2000). Type II myosin regulatory light chain relieves auto-inhibition of myosin-heavy-chain function. Nat Cell Biol *2*, 855-858. 10.1038/35041107.
19. Magliozzi, J.O., Sears, J., Cressey, L., Brady, M., Opalko, H.E., Kettenbach, A.N., and Moseley, J.B. (2020). Fission yeast Pak1 phosphorylates anillin-like Mid1 for spatial control of cytokinesis. J Cell Biol *219*. 10.1083/jcb.201908017.
20. Loo, T.H., and Balasubramanian, M. (2008). Schizosaccharomyces pombe Pak-related protein, Pak1p/Orb2p, phosphorylates myosin regulatory light chain to inhibit cytokinesis. J Cell Biol *183*, 785-793. 10.1083/jcb.200806127.

21. Pollard, L.W., Bookwalter, C.S., Tang, Q., Krementsova, E.B., Trybus, K.M., and Lowey, S. (2017). Fission yeast myosin Myo2 is down-regulated in actin affinity by light chain phosphorylation. Proc Natl Acad Sci U S A *114*, E7236-e7244. 10.1073/pnas.1703161114.
22. Prieto-Ruiz, F., Gómez-Gil, E., Martín-García, R., Perez-Diaz, A.J., Vicente-Soler, J., Franco, A., Soto, T., Pérez, P., Madrid, M., and Cansado, J. (2023). Myosin II regulatory light chain phosphorylation and formin availability modulate cytokinesis upon changes in carbohydrate metabolism. Elife *12*. 10.7554/eLife.83285.
23. Rhind, N., Chen, Z., Yassour, M., Thompson, D.A., Haas, B.J., Habib, N., Wapinski, I., Roy, S., Lin, M.F., Heiman, D.I., et al. (2011). Comparative functional genomics of the fission yeasts. Science *332*, 930-936. 10.1126/science.1203357.
24. Aoki, K., Furuya, K., and Niki, H. (2017). Schizosaccharomyces japonicus: A Distinct Dimorphic Yeast among the Fission Yeasts. Cold Spring Harb Protoc *2017*, pdb.top082651. 10.1101/pdb.top082651.
25. Aoki, K., Hayashi, H., Furuya, K., Sato, M., Takagi, T., Osumi, M., Kimura, A., and Niki, H. (2011). Breakage of the nuclear envelope by an extending mitotic nucleus occurs during anaphase in Schizosaccharomyces japonicus. Genes Cells *16*, 911-926. 10.1111/j.1365-2443.2011.01540.x.
26. Yam, C., He, Y., Zhang, D., Chiam, K.H., and Oliferenko, S. (2011). Divergent strategies for controlling the nuclear membrane satisfy geometric constraints during nuclear division. Curr Biol *21*, 1314-1319. 10.1016/j.cub.2011.06.052.
27. Gu, Y., Yam, C., and Oliferenko, S. (2012). Divergence of mitotic strategies in fission yeasts. Nucleus *3*, 220-225. 10.4161/nucl.19514.
28. Yam, C., Gu, Y., and Oliferenko, S. (2013). Partitioning and remodeling of the Schizosaccharomyces japonicus mitotic nucleus require chromosome tethers. Curr Biol *23*, 2303-2310. 10.1016/j.cub.2013.09.057.
29. Kaino, T., Tonoko, K., Mochizuki, S., Takashima, Y., and Kawamukai, M. (2018). Schizosaccharomyces japonicus has low levels of CoQ(10) synthesis, respiration deficiency, and efficient ethanol production. Biosci Biotechnol Biochem *82*, 1031-1042. 10.1080/09168451.2017.1401914.
30. Sipiczki, M., Takeo, K., Yamaguchi, M., Yoshida, S., and Miklos, I. (1998). Environmentally controlled dimorphic cycle in a fission yeast. Microbiology *144 (Pt 5)*, 1319-1330. 10.1099/00221287-144-5-1319.
31. Papp, L., Sipiczki, M., Holb, I.J., and Miklos, I. (2014). Optimal conditions for mycelial growth of Schizosaccharomyces japonicus cells in liquid medium: it enables the molecular investigation of dimorphism. Yeast *31*, 475-482. 10.1002/yea.3048.
32. Niki, H. (2017). Induction of Hyphal Growth in Schizosaccharomyces japonicus. Cold Spring Harb Protoc *2017*, pdb.prot091868. 10.1101/pdb.prot091868.
33. Kinnaer, C., Dudin, O., and Martin, S.G. (2019). Yeast-to-hypha transition of Schizosaccharomyces japonicus in response to environmental stimuli. Mol Biol Cell *30*, 975-991. 10.1091/mbc.E18-12-0774.
34. Gu, Y., Yam, C., and Oliferenko, S. (2015). Rewiring of cellular division site selection in evolution of fission yeasts. Curr Biol *25*, 1187-1194. 10.1016/j.cub.2015.02.056.
35. Furuya, K., and Niki, H. (2010). The DNA damage checkpoint regulates a transition between yeast and hyphal growth in Schizosaccharomyces japonicus. Mol Cell Biol *30*, 2909-2917. 10.1128/mcb.00049-10.
36. Berg, S., Kutra, D., Kroeger, T., Straehle, C.N., Kausler, B.X., Haubold, C., Schiegg, M., Ales, J., Beier, T., Rudy, M., et al. (2019). ilastik: interactive machine learning for (bio)image analysis. Nat Methods *16*, 1226-1232. 10.1038/s41592-019-0582-9.
37. Papp, L.A., Ács-Szabó, L., Póliska, S., and Miklós, I. (2021). A modified culture medium and hyphae isolation method can increase quality of the RNA extracted from mycelia of a dimorphic fungal species. Curr Genet *67*, 823-830. 10.1007/s00294-021-01181-4.
38. McCollum, D., Balasubramanian, M.K., Pelcher, L.E., Hemmingsen, S.M., and Gould, K.L. (1995). Schizosaccharomyces pombe cdc4+ gene encodes a novel EF-hand protein essential for cytokinesis. J Cell Biol *130*, 651-660. 10.1083/jcb.130.3.651.
39. Wang, S., Li, W., Liu, S., and Xu, J. (2016). RaptorX-Property: a web server for protein structure property prediction. Nucleic Acids Res *44*, W430-435. 10.1093/nar/gkw306.
40. Jumper, J., Evans, R., Pritzel, A., Green, T., Figurnov, M., Ronneberger, O., Tunyasuvunakool, K., Bates, R., Žídek, A., Potapenko, A., et al. (2021). Highly accurate protein structure prediction with AlphaFold. Nature *596*, 583-589. 10.1038/s41586-021-03819-2.
41. Kast, D., Espinoza-Fonseca, L.M., Yi, C., and Thomas, D.D. (2010). Phosphorylation-induced structural changes in smooth muscle myosin regulatory light chain. Proc Natl Acad Sci U S A *107*, 8207-8212. 10.1073/pnas.1001941107.
42. Steinberg, G., Peñalva, M.A., Riquelme, M., Wösten, H.A., and Harris, S.D. (2017). Cell Biology of Hyphal Growth. Microbiol Spectr *5*. 10.1128/microbiolspec.FUNK-0034-2016.
43. Sipiczki, M., Takeo, K., and Grallert, A. (1998). Growth polarity transitions in a dimorphic fission yeast. Microbiology *144 (Pt 12)*, 3475-3485. 10.1099/00221287-144-12-3475.
44. Moseley, J.B. (2015). Cytokinesis: does Mid1 have an identity crisis? Curr Biol *25*, R364-366. 10.1016/j.cub.2015.03.017.

45. Scarff, C.A., Carrington, G., Casas-Mao, D., Chalovich, J.M., Knight, P.J., Ranson, N.A., and Peckham, M. (2020). Structure of the shutdown state of myosin-2. Nature *588*, 515-520. 10.1038/s41586-020-2990-5.
46. Yang, S., Tiwari, P., Lee, K.H., Sato, O., Ikebe, M., Padrón, R., and Craig, R. (2020). Cryo-EM structure of the inhibited (10S) form of myosin II. Nature *588*, 521-525. 10.1038/s41586-020-3007-0.
47. Heissler, S.M., Arora, A.S., Billington, N., Sellers, J.R., and Chinthalapudi, K. (2021). Cryo-EM structure of the autoinhibited state of myosin-2. Sci Adv *7*, eabk3273. 10.1126/sciadv.abk3273.
48. McDonald, N.A., Lind, A.L., Smith, S.E., Li, R., and Gould, K.L. (2017). Nanoscale architecture of the Schizosaccharomyces pombe contractile ring. Elife *6*. 10.7554/eLife.28865.
49. Prieto-Ruiz, F., Vicente-Soler, J., Franco, A., Gomez-Gil, E., Sanchez-Marinas, M., Vazquez-Marin, B., Aligue, R., Madrid, M., Moreno, S., Soto, T., and Cansado, J. (2020). RNA-Binding Protein Rnc1 Regulates Cell Length at Division and Acute Stress Response in Fission Yeast through Negative Feedback Modulation of the Stress-Activated Mitogen-Activated Protein Kinase Pathway. mBio *11*. 10.1128/mBio.02815-19.
50. Petersen, J., and Russell, P. (2016). Growth and the Environment of Schizosaccharomyces pombe. Cold Spring Harb Protoc *2016*, pdb.top079764. 10.1101/pdb.top079764.
51. Aoki, K., and Niki, H. (2017). Transformation of Schizosaccharomyces japonicus. Cold Spring Harb Protoc *2017*, pdb.prot091850. 10.1101/pdb.prot091850.
52. Hentges, P., Van Driessche, B., Tafforeau, L., Vandenhaute, J., and Carr, A.M. (2005). Three novel antibiotic marker cassettes for gene disruption and marker switching in Schizosaccharomyces pombe. Yeast *22*, 1013-1019. 10.1002/yea.1291.
53. Sato, M., Dhut, S., and Toda, T. (2005). New drug-resistant cassettes for gene disruption and epitope tagging in Schizosaccharomyces pombe. Yeast *22*, 583-591. 10.1002/yea.1233.
54. Madrid, M., Soto, T., Khong, H., Franco, A., Vicente, J., Perez, P., Gacto, M., and Cansado, J. (2006). Stress-induced response, localization, and regulation of the Pmk1 cell integrity pathway in Schizosaccharomyces pombe. Journal of Biological Chemistry *281*, 2033-2043. 10.1074/jbc.M506467200.
55. Grallert, A., and Hagan, I.M. (2017). Preparation of Protein Extracts from Schizosaccharomyces pombe Using Trichloroacetic Acid Precipitation. Cold Spring Harb Protoc *2017*. 10.1101/pdb.prot091579.
56. Schneider, C., Rasband, W., and Eliceiri, K. (2012). NIH Image to ImageJ: 25 years of image analysis. Nature Methods *9*, 671-675. 10.1038/nmeth.2089.
57. Gómez-Gil, E., Martín-García, R., Vicente-Soler, J., Franco, A., Vázquez-Marín, B., Prieto-Ruiz, F., Soto, T., Pérez, P., Madrid, M., and Cansado, J. (2020). Stress-activated MAPK signalling controls fission yeast actomyosin ring integrity by modulating formin For3 levels. Elife *9*. 10.7554/eLife.57951.
58. Hagan, I.M. (2016). Immunofluorescence Microscopy of Schizosaccharomyces pombe Using Chemical Fixation. Cold Spring Harb Protoc *2016*. 10.1101/pdb.prot091017.

Key resources table

REAGENT or RESOURCE	SOURCE	IDENTIFIER
Antibodies		
anti-GFP (mouse monoclonal)	Roche	Cat# 11 814 460 001, RRID:AB_390913
anti-Cdk1/Cdc2 (PSTAIR)(rabbit polyclonal)	Millipore	Cat#: 06–923; RRID:AB_310302
anti-Mouse IgG- peroxidase (goat polyclonal)	Sigma Aldrich	Cat#: A5278; RRID:AB_258232
anti-Rabbit IgG- peroxidase (goat polyclonal)	Sigma Aldrich	Cat#: A6667; RRID:AB_258307
Chemicals, peptides, and recombinant proteins		
PhosTag acrylamide	Wako Chemical	Cat#: 300–93523
Alexa fluor 488-conjugated phalloidin	Thermo Fischer Scientific	Cat#: A12379
TCA	Sigma Aldrich	Cat#: 102134749
Glycerol	ERBA Pharm	Cat#: 346165
Soybean lectin	Sigma Aldrich	Cat#: L2650
Potassium Chloride	Panreac	Cat#:7447-40-7
Agarose	Pronadisa	Cat#: 8010.00
Red Grape Extract	Laboratory made	Kinnaer et al., 2019
Malt Extract	Milipore	Cat#: VM835891
Gelatin	Royal	Cat#: 1825133
Calcofluor White	Sigma Aldrich	Cat#: 1002046319
Camptotecin	Sigma Aldrich	Cat#: C9911
Critical commercial assays		
ECL Western Blotting Reagents	GE-Healthcare	Cat#: RPN2106
NEBuilder HiFi DNA Assembly Kit	New England Biolabs	Cat#: E2621L
Deposited data		
Raw Data of Figures	Mendeley	https://doi.org/10.17632/g9vv6xv4ct.1
AlphaFold2 Structures	Mendeley	https://doi.org/10.17632/g9vv6xv4ct.1
Experimental models: Organisms/strains		
S. pombe and *S. japonicus* strains	See Table S1	N/A
Oligonucleotides		
Oligonucleotides	See Table S2	N/A
Recombinant DNA		
pFA6a-GFP(S65T)::natMX6	Bälher et al., 1998	pFA6a-GFP(S65T)::natMX6
pJK210Rlc1Sp-GFP	This study	pJK210Rlc1Sp-GFP
pJK210Rlc1(S35A)Sp-GFP	This study	pJK210Rlc1(S35A)Sp-GFP
pJK210Rlc1(S35D)Sp-GFP	This study	pJK210Rlc1(S35D)Sp-GFP
pJK210Rlc1Sj-GFP	This study	pJK210Rlc1Sj-GFP

pJK210Rlc1(N23S)Sj-GFP	This study	pJK210Rlc1(N23S)Sj-GFP
pJK210Rlc1(Δ19-33)Sp-GFP	This study	pJK210Rlc1(Δ19-33)Sp-GFP
pJK210Rlc1(Δ19-33, S20A)Sp-GFP	This study	pJK210Rlc1(Δ19-33, S20A)Sp-GFP
pJK210Rlc1(NtermSj)Sp-GFP	This study	pJK210Rlc1(NtermSj)Sp-GFP
pJK210Rlc1(T104WS108W)Sp-GFP	This study	pJK210Rlc1(T104WS108W)Sp-GFP
pJK210Rlc1(S35AT104WS108W)Sp-GFP	This study	pJK210Rlc1(S35AT104WS108W)Sp-GFP
pFA6a::natMX6	Bälher et al., 1998	pFA6a::natMX6
pSLRlc1Sj-GFP	This study	pSLRlc1Sj-GFP
pSLRlc1(N23S)Sj-GFP	This study	pSLRlc1(N23S)Sj-GFP
pSLRlc1Sp-GFP	This study	pSLRlc1Sp-GFP
pSLRlc1(S35A)Sp-GFP	This study	pSLRlc1(S35A)Sp-GFP
Software and algorithms		
ImageJ	Schneider et al., 2012	https://imagej.net/software/fiji/
Graphpad Prism 9.0.2	Graphpad Software	https://www.graphpad.com
Alphafold2	Jumper et al., 2021	https://colab.research.google.com/github/sokrypton/ColabFold/blob/main/AlphaFold2.ipynb
PyMol	Jumper et al., 2021	https://pymol.org/2
RaptorX	Wang et al., 2016	https://bio.tools/raptorx
ClustalW	ClustalW Software	https://www.ebi.ac.uk/Tools/msa/clustalo/
BioRender	BioRender Software	https://www.biorender.com
Ilastik	Berg et al., 2019	https://www.ilastik.org/
Other		
µ-Slide 8 well	Ibidi	Cat#: 80826

Figure 1

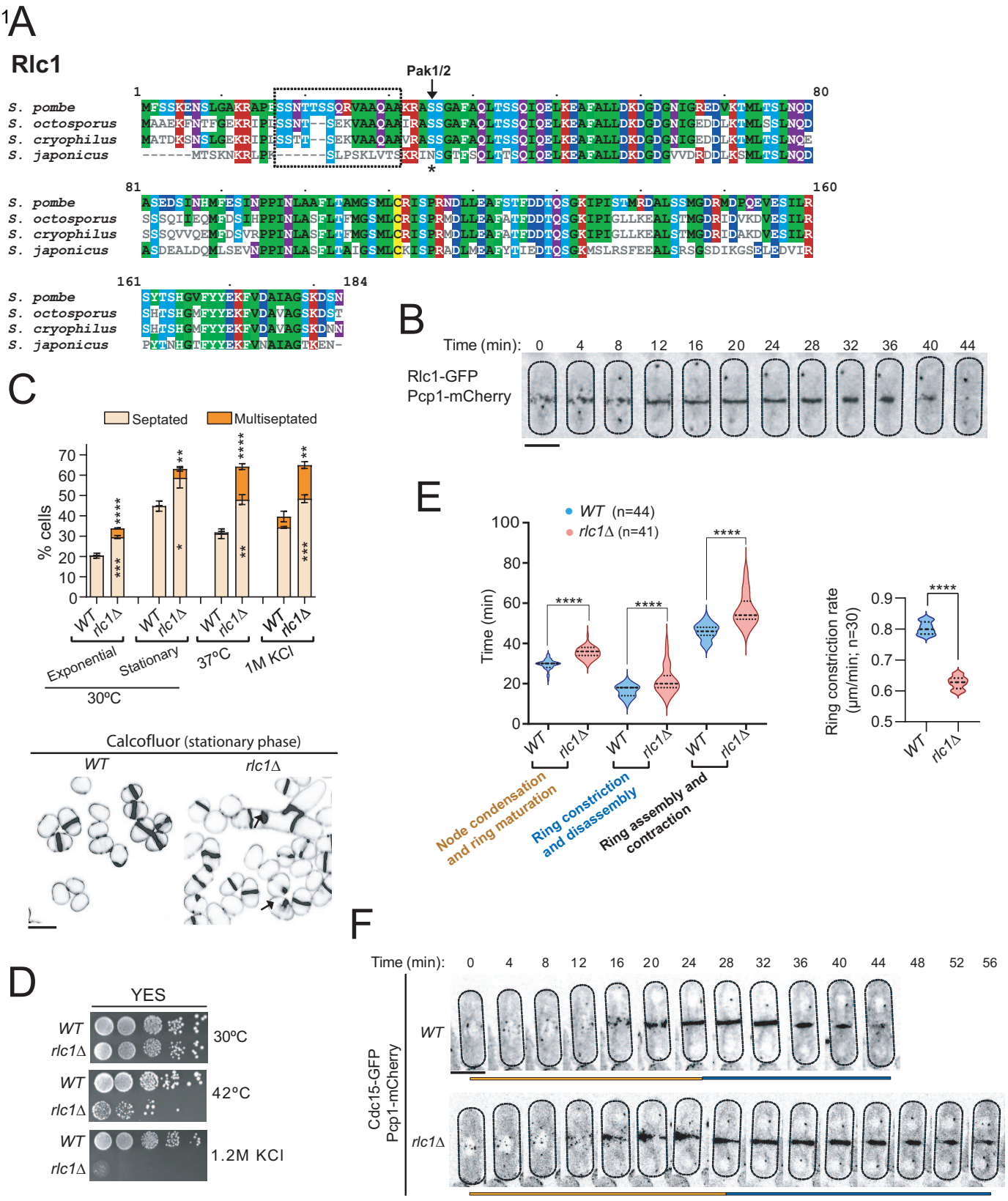
A
Rlc1
Pak1/2
S. pombe
S. octosporus
S. cryophilus
S. japonicus
B
Time (min): 0 4 8 12 16 20 24 28 32 36 40 44
Rlc1-GFP
Pcp1-mCherry
C
Septated
Multiseptated
% cells
WT
rlc1Δ
Exponential
Stationary
37°C
1M KCl
30°C
Calcofluor (stationary phase)
D
YES
30°C
42°C
1.2M KCl
E
WT (n=44)
rlc1Δ (n=41)
Time (min)
Node condensation and ring maturation
Ring constriction and disassembly
Ring assembly and contraction
Ring constriction rate (μm/min; n=30)
F
Time (min): 0 4 8 12 16 20 24 28 32 36 40 44 48 52 56
Cdc15-GFP
Pcp1-mCherry

Figure 2

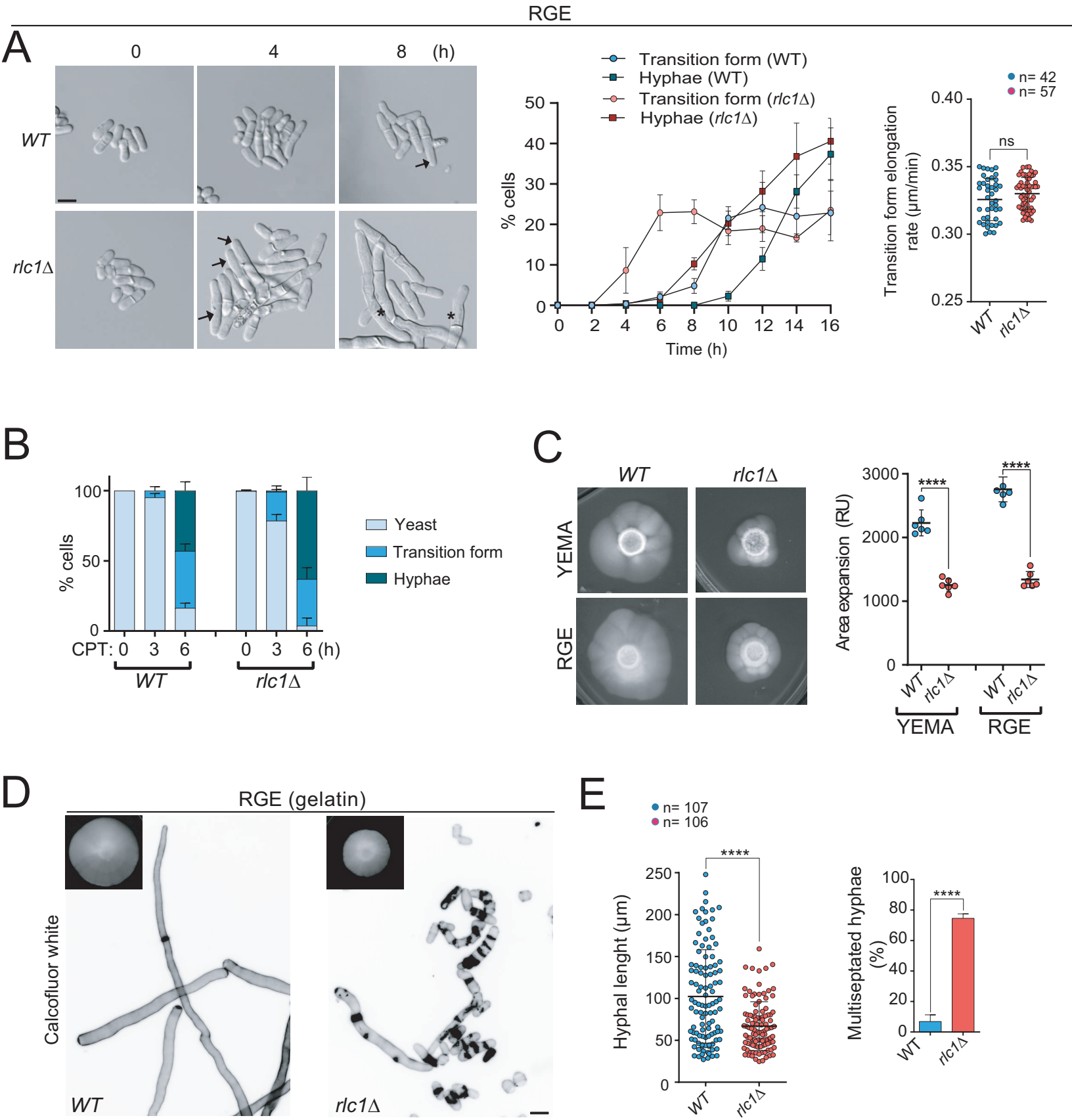
RGE
A
0
4
8 (h)
WT
rlc1Δ
Transition form (WT)
Hyphae (WT)
Transition form (rlc1Δ)
Hyphae (rlc1Δ)
% cells
Time (h)
n= 42
n= 57
ns
Transition form elongation rate (µm/min)
B
% cells
Yeast
Transition form
Hyphae
CPT: 0 3 6 0 3 6 (h)
WT
rlc1Δ
C
WT
rlc1Δ
YEMA
RGE
Area expansion (RU)
****
YEMA
RGE
D
RGE (gelatin)
Calcofluor white
WT
rlc1Δ
E
n= 107
n= 106
Hyphal lenght (µm)
Multiseptated hyphae (%)

Figure

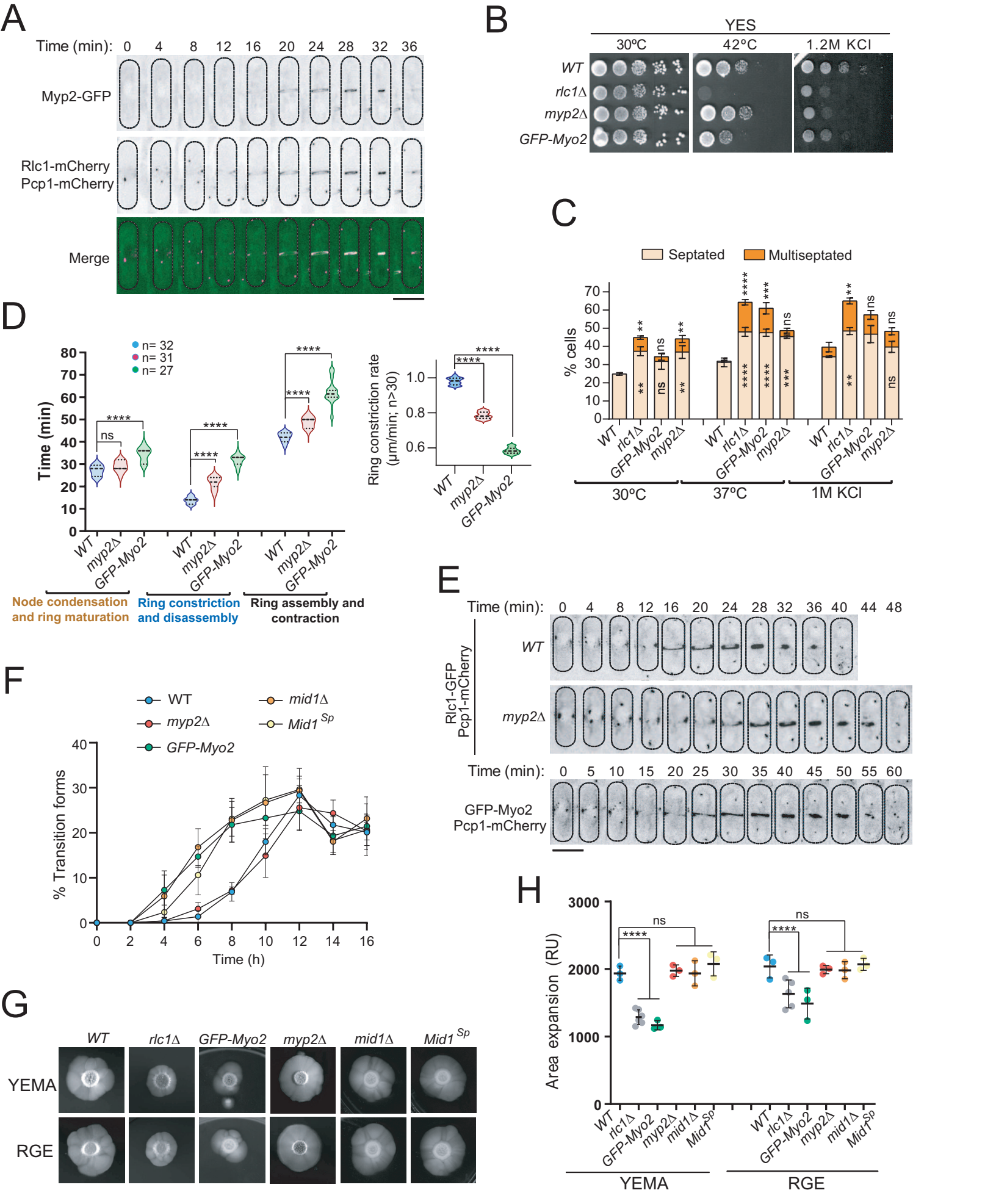
A
Time (min): 0 4 8 12 16 20 24 28 32 36
Myp2-GFP
Rlc1-mCherry
Pcp1-mCherry
Merge
B
YES
30ºC
42ºC
1.2M KCl
WT
rlc1Δ
myp2Δ
GFP-Myo2
C
Septated
Multiseptated
% cells
30ºC
37ºC
1M KCl
D
n= 32
n= 31
n= 27
Time (min)
Ring constriction rate (µm/min; n>30)
Node condensation and ring maturation
Ring constriction and disassembly
Ring assembly and contraction
E
Time (min): 0 4 8 12 16 20 24 28 32 36 40 44 48
Rlc1-GFP Pcp1-mCherry
Time (min): 0 5 10 15 20 25 30 35 40 45 50 55 60
GFP-Myo2 Pcp1-mCherry
F
WT
myp2Δ
GFP-Myo2
mid1Δ
Mid1 Sp
% Transition forms
Time (h)
G
WT
rlc1Δ
GFP-Myo2
myp2Δ
mid1Δ
Mid1 Sp
YEMA
RGE
H
Area expansion (RU)
YEMA
RGE

Figure 4

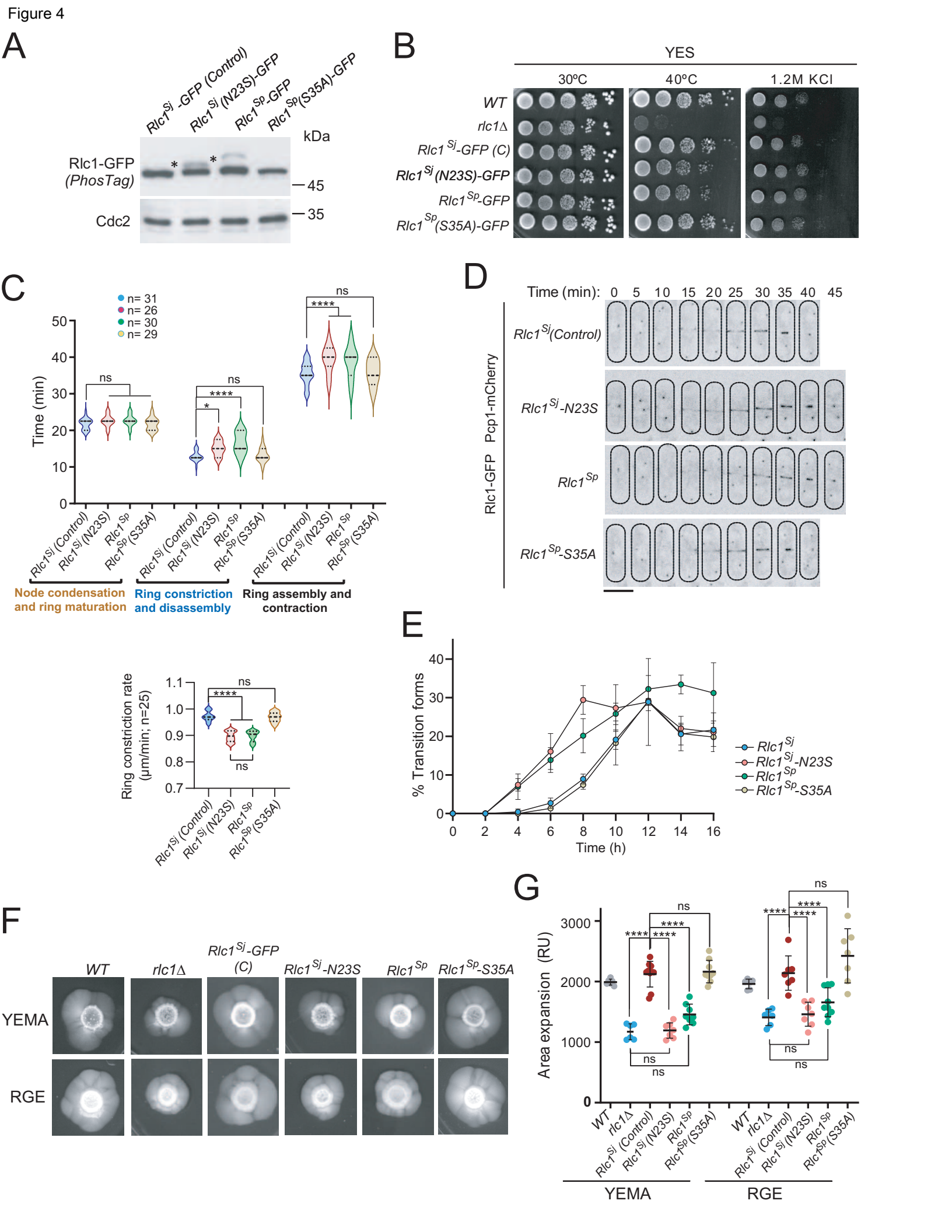
A
Rlc1Sj -GFP (Control)
Rlc1Sj (N23S)-GFP
Rlc1Sp-GFP
Rlc1Sp(S35A)-GFP
kDa
Rlc1-GFP (PhosTag)
45
Cdc2
35
B
YES
30ºC
40ºC
1.2M KCl
WT
rlc1Δ
Rlc1Sj-GFP (C)
Rlc1Sj (N23S)-GFP
Rlc1Sp-GFP
Rlc1Sp(S35A)-GFP
C
n= 31
n= 26
n= 30
n= 29
Time (min)
ns
****
*
Rlc1Sj (Control)
Rlc1Sj (N23S)
Rlc1Sp
Rlc1Sp (S35A)
Node condensation and ring maturation
Ring constriction and disassembly
Ring assembly and contraction
D
Time (min): 0 5 10 15 20 25 30 35 40 45
Rlc1-GFP Pcp1-mCherry
Rlc1Sj(Control)
Rlc1Sj-N23S
Rlc1Sp
Rlc1Sp-S35A
Ring constriction rate (µm/min; n=25)
E
% Transition forms
Time (h)
Rlc1Sj
Rlc1Sj-N23S
Rlc1Sp
Rlc1Sp-S35A
F
WT
rlc1Δ
Rlc1Sj-GFP (C)
Rlc1Sj-N23S
Rlc1Sp
Rlc1Sp-S35A
YEMA
RGE
G
Area expansion (RU)
YEMA
RGE

Figure 5

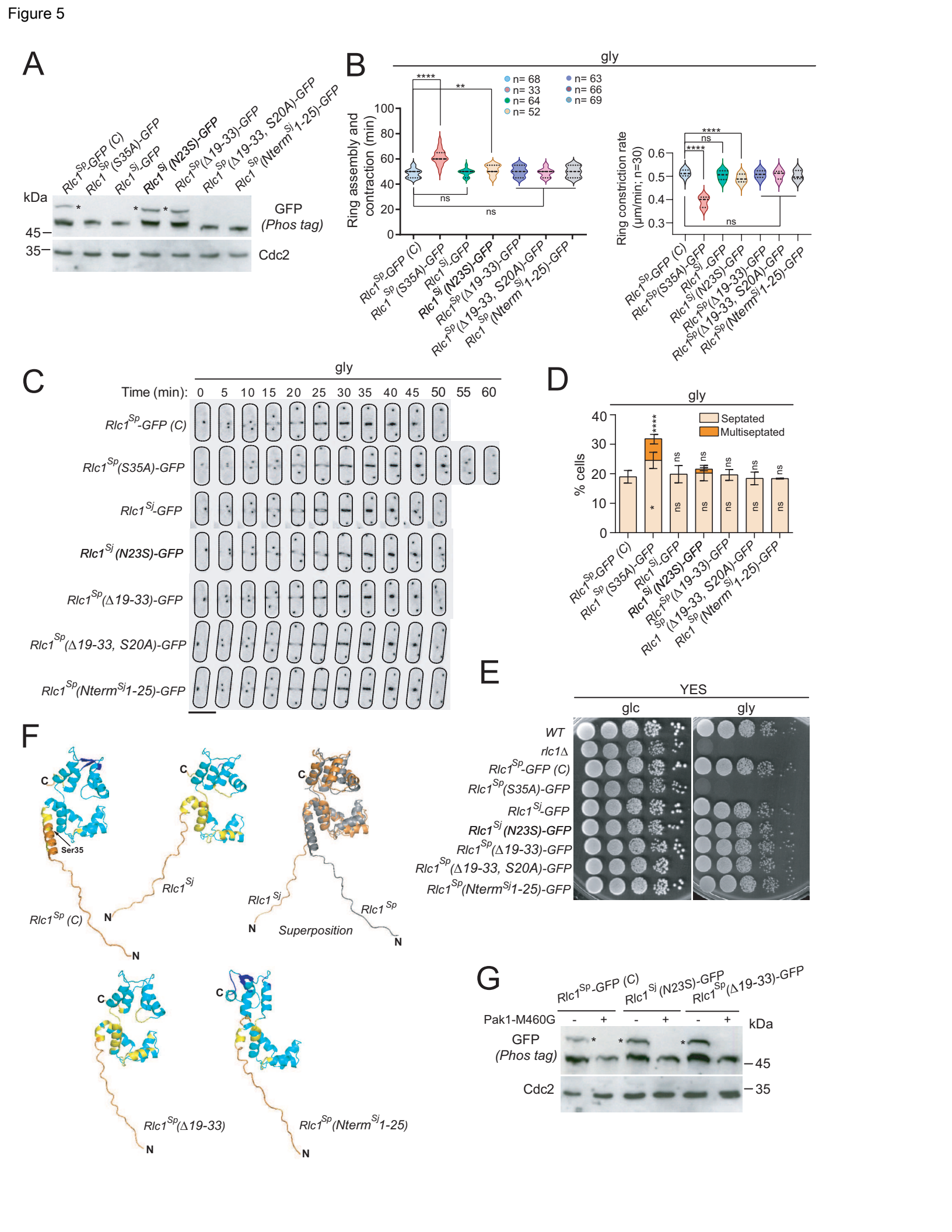
A
Rlc1Sp-GFP (C)
Rlc1Sp(S35A)-GFP
Rlc1Sj-GFP
Rlc1Sj (N23S)-GFP
Rlc1Sp(Δ19-33)-GFP
Rlc1Sp(Δ19-33, S20A)-GFP
Rlc1Sp(Nterm Sj1-25)-GFP
kDa
45
35
GFP (Phos tag)
Cdc2
B
gly
Ring assembly and contraction (min)
n= 68
n= 33
n= 64
n= 52
n= 63
n= 66
n= 69
****
**
ns
Ring constriction rate (μm/min; n=30)
C
gly
Time (min): 0 5 10 15 20 25 30 35 40 45 50 55 60
Rlc1Sp-GFP (C)
Rlc1Sp(S35A)-GFP
Rlc1Sj-GFP
Rlc1Sj (N23S)-GFP
Rlc1Sp(Δ19-33)-GFP
Rlc1Sp(Δ19-33, S20A)-GFP
Rlc1Sp(NtermSj1-25)-GFP
D
gly
% cells
Septated
Multiseptated
E
YES
glc
gly
WT
rlc1Δ
Rlc1Sp-GFP (C)
Rlc1Sp(S35A)-GFP
Rlc1Sj-GFP
Rlc1Sj (N23S)-GFP
Rlc1Sp(Δ19-33)-GFP
Rlc1Sp(Δ19-33, S20A)-GFP
Rlc1Sp(NtermSj1-25)-GFP
F
C
N
Ser35
Rlc1Sp (C)
Rlc1Sj
Superposition
Rlc1Sp(Δ19-33)
Rlc1Sp(NtermSj1-25)
G
Rlc1Sp-GFP (C)
Rlc1Sj (N23S)-GFP
Rlc1Sp(Δ19-33)-GFP
Pak1-M460G
kDa
GFP (Phos tag)
Cdc2
45
35

Figure 6

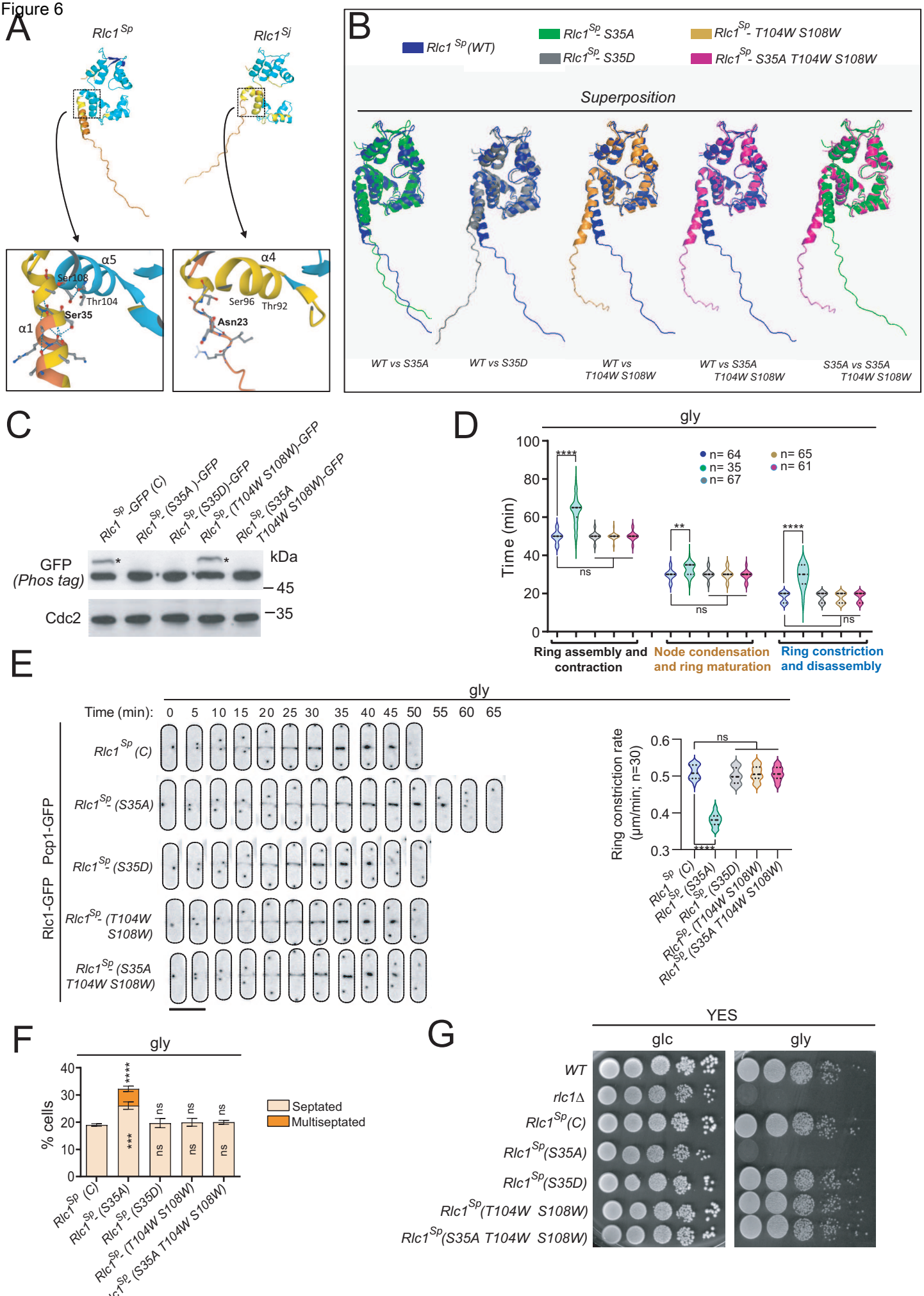
A
Rlc1 Sp
Rlc1 Sj
α5
Ser108
Thr104
Ser35
α1
α4
Ser96
Thr92
Asn23
B
Rlc1 Sp (WT)
Rlc1 Sp- S35A
Rlc1 Sp- S35D
Rlc1 Sp- T104W S108W
Rlc1 Sp- S35A T104W S108W
Superposition
WT vs S35A
WT vs S35D
WT vs T104W S108W
WT vs S35A T104W S108W
S35A vs S35A T104W S108W
C
Rlc1 Sp -GFP (C)
Rlc1 Sp- (S35A)-GFP
Rlc1 Sp- (S35D)-GFP
Rlc1 Sp- (T104W S108W)-GFP
Rlc1 Sp- (S35A T104W S108W)-GFP
GFP (Phos tag)
Cdc2
kDa
45
35
D
gly
Time (min)
n= 64
n= 35
n= 67
n= 65
n= 61
****
**
ns
Ring assembly and contraction
Node condensation and ring maturation
Ring constriction and disassembly
E
gly
Time (min): 0 5 10 15 20 25 30 35 40 45 50 55 60 65
Rlc1-GFP Pcp1-GFP
Rlc1 Sp (C)
Rlc1 Sp- (S35A)
Rlc1 Sp- (S35D)
Rlc1 Sp- (T104W S108W)
Rlc1 Sp- (S35A T104W S108W)
Ring constriction rate (μm/min; n=30)
F
gly
% cells
Septated
Multiseptated
G
YES
glc
gly
WT
rlc1Δ
Rlc1 Sp(C)
Rlc1 Sp(S35A)
Rlc1 Sp(S35D)
Rlc1 Sp(T104W S108W)
Rlc1 Sp(S35A T104W S108W)

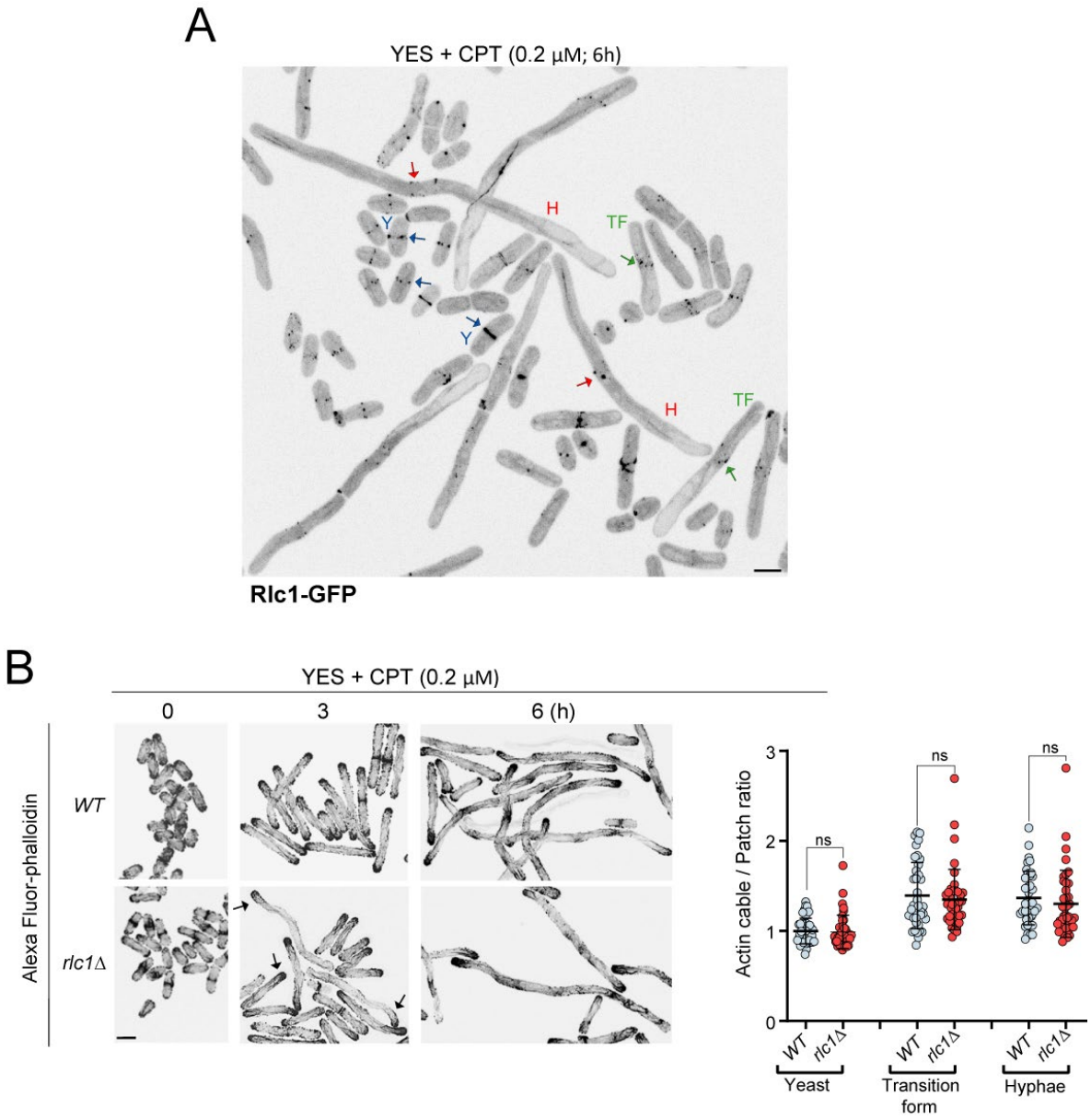

Figure S1. Interphase Rlc1^{Sj} nodes negatively regulates the onset of *S. japonicus* yeast to hypha differentiation. Related to Figure 2.

(A) Representative maximum-projection time-lapse image of *S. japonicus* wild-type cells expressing a genomic Rlc1-GFP fusion and grown in YES medium supplemented with 0.2 µM CPT for 6 h. Arrows indicate the presence of equatorial Rlc1 nodes at interphase cells and the CAR in yeast (Y), transition forms (TF) and hyphae (H). Scale bar: 10 µm.

(B) Left: Representative maximum projection images of Alexa Fluor phalloidin-stained *S. japonicus* cells grown in YES medium supplemented with 0.2 µM CPT for the indicated times. Arrows: transition forms. Scale bar: 10 µm. Right: Segmentation analysis using the Ilastik routine. Quantification data correspond to the actin cable to patch ratio of yeast, transition forms and hyphae (n=40 for each cell type) and are presented as mean relative units ± SD. ns, not significant, as calculated by unpaired Student's t-test.

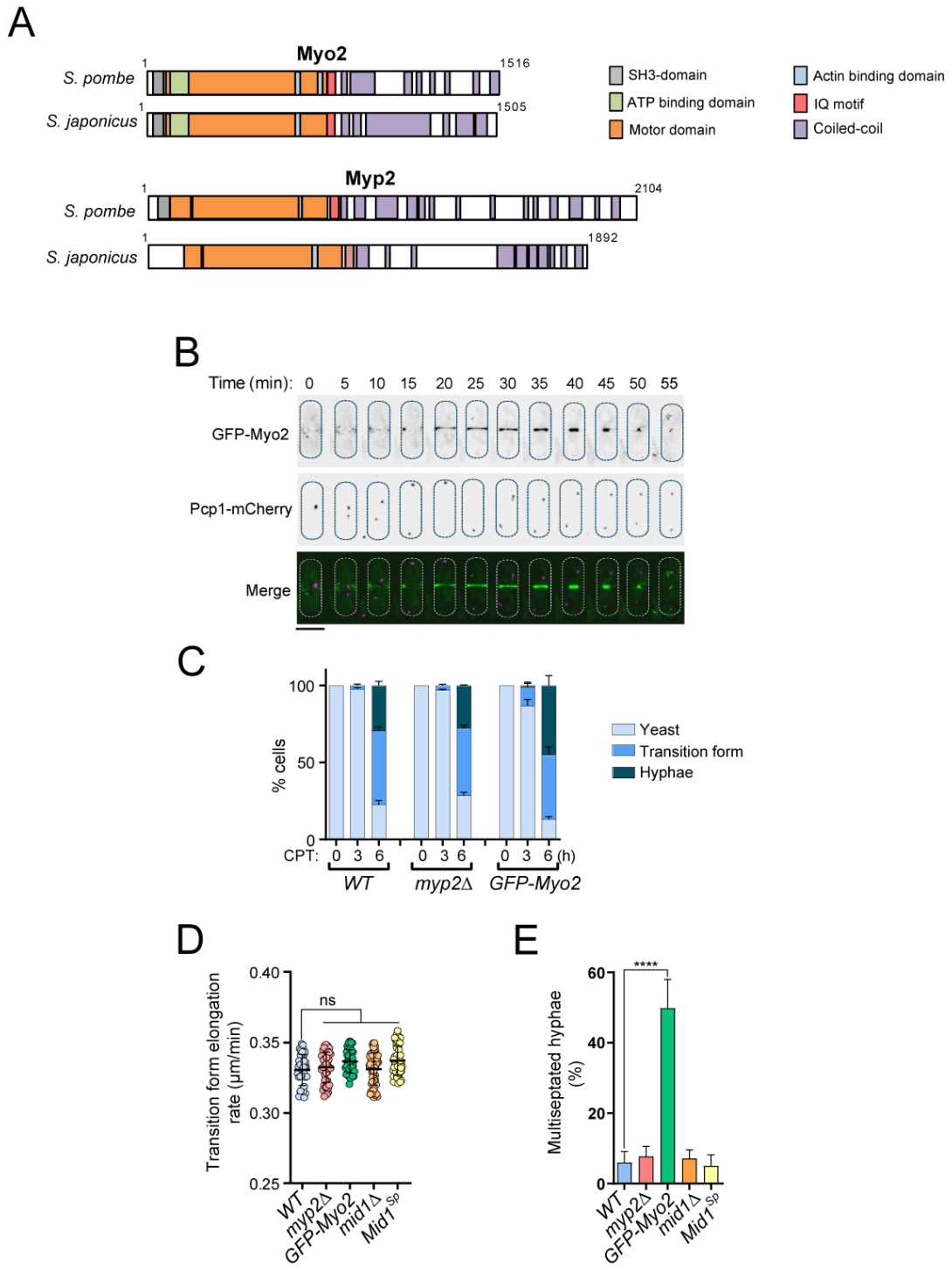

Figure S2. Roles of Myo2^{Sj} and Myp2^{Sj} during cytokinesis and yeast to hypha dimorphism. Related to Figure 3.
(A) Organization and domain conservation of myosin-II isoforms in *S. pombe* and *S. japonicus*. Motor, ATPase and actin-binding domains, IQ motifs (regulatory light chain (RLC) binding site) and coiled-coil regions are shown.
(B) Maximum-projection time-lapse images of GFP-Myo2 dynamics at the equatorial region of cells growing in YES-glucose. Mitotic progression was monitored using Pcp1-mCherry-labeled SPBs. Scale bar: 10 µm.
(C) The percentages of yeasts, transition forms and hyphae were determined in the indicated strains during incubation in YES-glucose medium supplemented with 0.2 µM. Data correspond to three independent experiments and are presented as mean ± SD.
(D) Elongation rates of transition forms (µm/min) were determined for the indicated strains. Cells (n≥38) were scored from three independent experiments, and data are presented as scatter plots. Statistical comparison between two groups was performed by one-way ANOVA. ns, not significant.
(E) The percentage of multiseptated hyphae was quantified. Data correspond to three independent experiments and are presented as mean ± SD. ****, P<0.0001, as calculated by unpaired Student's t-test.

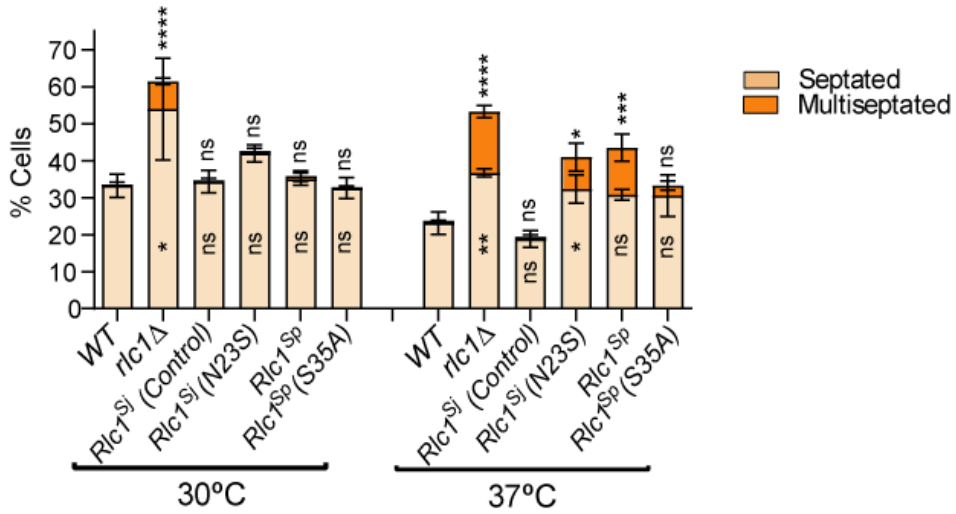

Figure S3. Misregulation of Myo2^{Sj} activity by Rlc1 phosphorylation elicits a multiseptated phenotype in *S. japonicus*. Related to Figure 4.

Strains of the indicated genotypes were grown in YES-glucose medium and incubated at 30ºC and 37ºC, and the percentage of septated and multiseptated cells were quantified. Data correspond to three independent experiments and are presented as mean ± SD. Statistical comparison was performed by one-way ANOVA. ****, $p<0.0001$; ***, $p<0.0005$; **, $p<0.005$; ns, not significant.

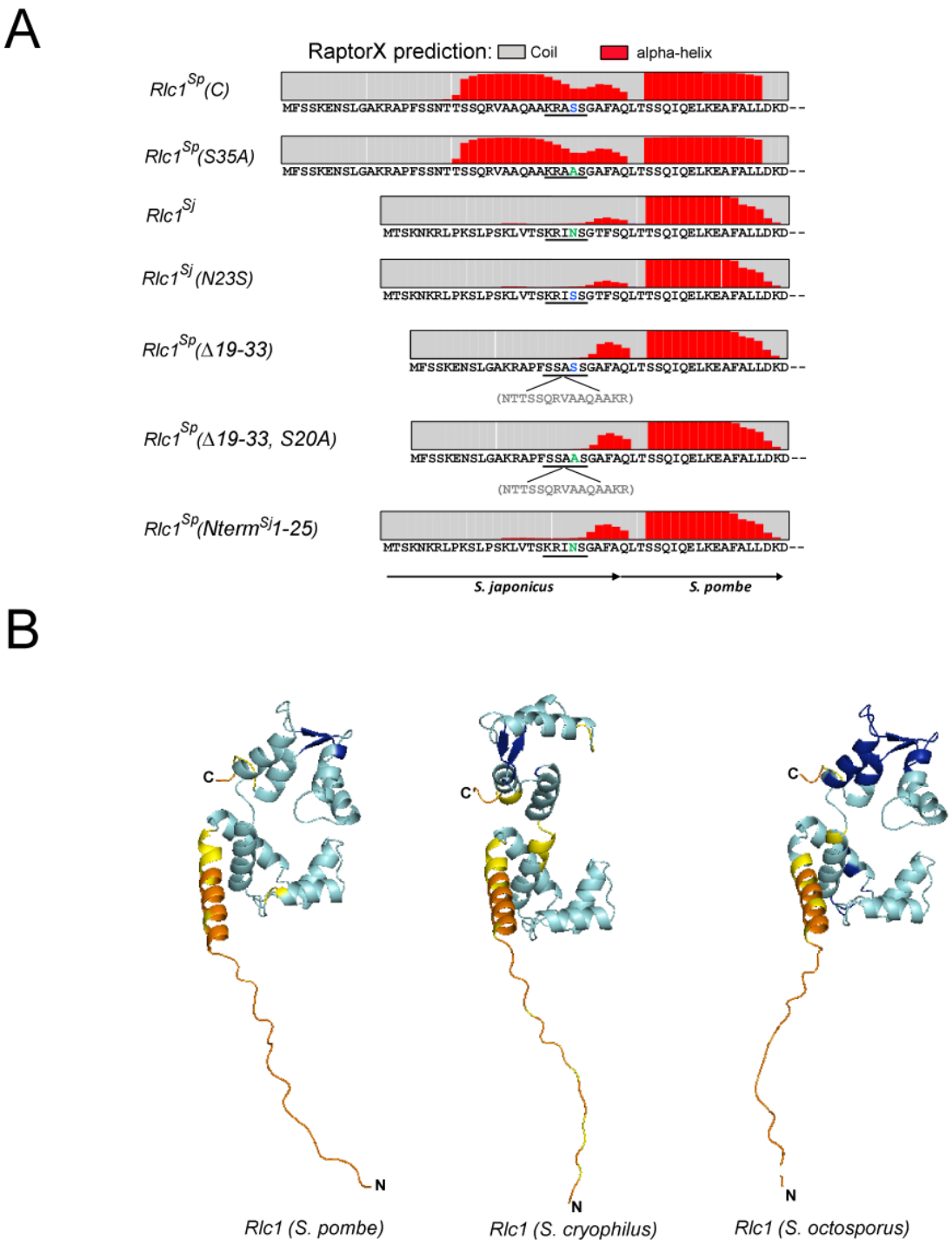

Figure S4. Prediction of secondary and 3D structures in fission yeast species. Related to Figure 5.
(A) Prediction of secondary structure in Rlc1^{Sp} and Rlc1^{Sj} wild type and mutant versions with RaptorX.
(B) AlphaFold2 prediction of wild-type Rlc1 versions in *S. pombe*, *S. cryophilus* and *S. octosporus*.

Table S1. *S. japonicus* and *S. pombe* strains used in this work. Related to Figures 1 to 6 and S1 to S3.

Reference	Genotype	Source
	Figure 1 (*S. japonicus*)	
DGG34	*h$^+$ pcp1-mCherry::kanMx6::ura4$^+$ rlc1-mCherry::kanMx6::ura4$^+$*	This work
NIG2017	*h$^+$ prototroph*	*Furuya & Niki, 2009*
DGG1	*h$^-$ rlc1::NatMx6 prototroph*	This work
DGG4	*h$^+$ pcp1-mCherry::kanMx6::ura4$^+$ cdc15-GFP::kanMx6::ura4$^+$*	This work
DGG7	*h$^+$ pcp1-mCherry::kanMx6::ura4$^+$ cdc15-GFP::kanMx6::ura4$^+$ rlc1::NatMx6*	This work
	Figure 2 (*S. japonicus*)	
NIG2017	*h$^+$ prototroph*	*Furuya & Niki, 2009*
DGG1	*h$^-$ rlc1::NatMx6 prototroph*	This work
	Figure 3 (*S. japonicus*)	
DGG36	*h$^+$ pcp1-mCherry::kanMx6::ura4$^+$ rlc1-mCherry::kanMx6::ura4$^+$ myp2-GFP::NatMx6*	This work
DGG8	*h$^+$ pcp1-mCherry::kanMx6::ura4$^+$ rlc1-GFP::kanMx6::ura4$^+$*	This work
DGG41	*h$^+$ pcp1-mCherry::kanMx6::ura4$^+$ rlc1-GFP::kanMx6::ura4$^+$ myp2::NatMx6*	This work
DGG45	*h$^+$ pcp1-mCherry::kanMx6::ura4$^+$ Myo2 promoter-GFP-myo2::ura4$^+$*	This work
NIG2017	*h$^+$ prototroph*	*Furuya & Niki, 2009*
DGG1	*h$^-$ rlc1::NatMx6 prototroph*	This work
SOJ1556	*h$^+$ Myo2 promoter-GFP-myo2::ura4$^+$*	*Gu et al., 2015*
DGG33	*h- myp2::NatMx6 prototroph*	This work
DGG47	*h$^+$ mid1::ura4$^+$*	This work
DGG51	*h- GFP-mid1(S.p)::KanMx6 prototroph*	This work
	Figure 4 (*S. japonicus*)	
DGG21	*h$^+$ rlc1::NatMx6 pcp1-mCherry::KanMx6::ura4$^+$ rlc1^{Sj}-GFP::ura4$^+$*	This work
DGG29	*h$^+$ rlc1::NatMx6 pcp1-mCherry::KanMx6::ura4$^+$ rlc1(N23S)^{Sj}-GFP::ura4$^+$*	This work
DGG25	*h$^+$ rlc1::NatMx6 pcp1-mCherry::KanMx6::ura4$^+$ rlc1^{Sp}-GFP::ura4$^+$*	This work
DGG31	*h$^+$ rlc1::NatMx6 pcp1-mCherry::KanMx6::ura4$^+$ rlc1(S35A)^{Sp}-GFP::ura4$^+$*	This work
	Figure 5 (*S. pombe*)	
FPR1704	*h$^+$ Pcp1-GFP:kanR rlc1::kanR Rlc1^{Sp}-GFP::ura4$^+$ ade6-M216 leu1-32*	This work
FPR1709	*h$^+$ Pcp1-GFP:kanR rlc1::kanR Rlc1(S35A)^{Sp}-GFP::ura4$^+$ ade6-M216 leu1-32*	This work
FPR1718	*h$^+$ Pcp1-GFP:kanR rlc1::kanR Rlc1^{Sj}-GFP::ura4$^+$ ade6-M216 leu1-32*	This work

FPR1724	*h⁺ Pcp1-GFP:kanR rlc1::kanR Rlc1(N23S)^{Sj}-GFP::ura4⁺ ade6-M216 leu1-32*	This work
FPR1741	*h⁺ Pcp1-GFP:kanR rlc1::kanR Rlc1(Δ19-33)^{Sp}-GFP::ura4⁺ ade6-M216 leu1-32*	This work
FPR1749	*h⁺ Pcp1-GFP:kanR rlc1::kanR Rlc1(Δ19-33,S20A)^{Sp}-GFP::ura4⁺ ade6-M216 leu1-32*	This work
FPR1730	*h⁺ Pcp1-GFP:kanR rlc1::kanR Rlc1Nterm^{Sj}-Rlc1(S35A)^{Sp}-GFP::ura4⁺ ade6-M216 leu1-32*	This work
	Figure 6 (*S. pombe*)	
FPR1704	*h⁺ Pcp1-GFP:kanR rlc1::kanR Rlc1^{Sp}-GFP::ura4⁺ ade6-M216 leu1-32*	This work
FPR1709	*h⁺ Pcp1-GFP:kanR rlc1::kanR Rlc1(S35A)^{Sp}-GFP::ura4⁺ ade6-M216 leu1-32*	This work
FPR1759	*h⁺ Pcp1-GFP:kanR rlc1::kanR Rlc1(S35D)^{Sp}-GFP::ura4⁺ ade6-M216 leu1-32*	This work
FPR1763	*h⁺ Pcp1-GFP:kanR rlc1::kanR Rlc1(T104WT108W)^{Sp}-GFP::ura4⁺ ade6-M216 leu1-32*	This work
FPR1767	*h⁺ Pcp1-GFP:kanR rlc1::kanR Rlc1(S35AT104WT108W)^{Sp}-GFP::ura4⁺ ade6-M216 leu1-32*	This work
	Figure S1 (*S. japonicus*)	
DGG21	*h⁺ rlc1::NatMx6 pcp1-mCherry::KanMx6::ura4⁺ rlc1^{Sj}-GFP::ura4⁺*	This work
NIG2017	*h⁺ prototroph*	*Furuya & Niki, 2009*
DGG1	*h⁻ rlc1::NatMx6 prototroph*	This work
	Figure S2 (*S. japonicus*)	
DGG45	*h⁺ pcp1-mCherry::kanMx6::ura4⁺ Myo2promoter-GFP-myo2::ura4⁺*	This work
NIG2017	*h⁺ prototroph*	*Furuya & Niki, 2009*
DGG1	*h⁻ rlc1::NatMx6 prototroph*	This work
SOJ1556	*h⁺ Myo2promoter-GFP-myo2::ura4⁺*	*Gu et al., 2015*
DGG33	*h- myp2::NatMx6 protrotroph*	This work
DGG47	*h⁺ mid1::ura4⁺*	This work
DGG51	*h- GFP-mid1(S.p)::KanMx6 prototroph*	This work
	Figure S3 (*S. japonicus*)	
DGG21	*h⁺ rlc1::NatMx6 pcp1-mCherry::KanMx6::ura4⁺ rlc1^{Sj}-GFP::ura4⁺*	This work
DGG29	*h⁺ rlc1::NatMx6 pcp1-mCherry::KanMx6::ura4⁺ rlc1(N23S)^{Sj}-GFP::ura4⁺*	This work
DGG25	*h⁺ rlc1::NatMx6 pcp1-mCherry::KanMx6::ura4⁺ rlc1^{Sp}-GFP::ura4⁺*	This work
DGG31	*h⁺ rlc1::NatMx6 pcp1-mCherry::KanMx6::ura4⁺ rlc1(S35A)^{Sp}-GFP::ura4⁺*	This work

Table S2. Oligonucleotides used in this work. Related to Figures 1 to 6 and S1 to S3.

Oligonucleotide	SEQUENCE 5'-3'	Use
Rlc1SjDel-F	ACACATCCCAGTTACCGTATCACGTTTATCTTCTTCCAGTGGTA CACGTTTTTTTACATACATTGGACCCGTTTAGCTTGCCTCGTC	*rlc1*$^{+Sj}$ deletion
Rlc1SjDel-R	GCTTTCATTTTGTTGTTGTCTTGTGTGAATATATGTCTCTGTGT GCCTGTTTGACATCACAAATTTAATTAAGCTATACAGATGGCG GCGTTAGTAT	*rlc1*$^{+Sj}$ deletion
Rlc1SjComp-F	AACAAGCAACTACAGTGCTGA	Confirmation of *rlc1*$^{+Sj}$ deletion
Myp2SjDel-F	TTATTCACTAGTGTTTACTACTCTCACAGCCTTCCGTTACTATG ACAACGATGTTTACTAAGTGGGACACGTTTAGCTTGCCTCGTC	*myp2*$^{+Sj}$ deletion
Myp2SjDel-R	TCGCGTTTTGCTTTAAATTTAAACTATGTGCAAACCGTGTCAG CAGGTCTATCGCGGTATTTGCAATTTGGCGGGCCTTAGATGGC GGCGTTAGTAT	*myp2*$^{+Sj}$ deletion and C-terminal tagging
Myp2SjTag-F	AGCGGAATGCCAAACTTCGCTTTCTCATGGATGATATTCACCA ACCTGATCGAACGTCTCGTTCGCTGGACTTTTCACCTATCCCC GGGTTAATTAA	*myp2*$^{+Sj}$ C-terminal tagging
Myp2Comp-F	ACGATTGTCCTCCTCTTTCTG	Confirmation of *myp2*$^{+Sj}$ deletion
Nat-Comp-REV	TTATTGTCAGTACTGATTAGGGGCA	Common oligonucleotide for confirmation of gene tagging
PromRlc1Sj-FWD	CCACCGCGGTGGCGGCCGCTCTAGAACTAGTGGATCCCCC TCCAGGAAGCAAGCGTACTTGATCC	*Rlc1*^{Sj}*-GFP* and *Rlc1*^{Sp}*-GFP* assembly in *S. japonicus*
PromRlc1Sj/Sj-REV	CGTTTGTTTTTTGAAGTCATGGGTCCAATGTATGTAAAAAAAC GTGTACC	*Rlc1*^{Sj}*-GFP* assembly in *S. japonicus*
Rlc1Sj-GFP-FWD	TTTTTACATACATTGGACCC ATGACTTCAAAAAACAAACGTCTCCCTAAAAG	*Rlc1*^{Sj}*-GFP* assembly in *S. japonicus*
Rlc1-GFP-REV	CGACGGTATCGATAAGCTTGATATCGAATTCCTGCAGCCC GCCGGTAGAGGTGTGGTCAATAAGAG	*Rlc1*^{Sj}*-GFP* and *Rlc1*^{Sp}*-GFP* assembly in *S. japonicus*
PromRlc1Sj/Sp-REV	TTTTCCTTCGAAGAGAACAT GGGTCCAATGTATGTAAAAAAACGTGTACC	*Rlc1*^{Sp}*-GFP* assembly in *S. japonicus*
Rlc1Sp-GFP-FWD	TTTTTACATACATTGGACCC ATGTTCTCTTCGAAGGAAAATTCCTTAGGTG	*Rlc1*^{Sp}*-GFP* assembly in *S. japonicus*
PromRlc1Sp-FWD	CGACGGTATCGATAAGCTTGATATCGAATTCCTGCAGCCCCAT ACTCCTTATTTCCTTCATTCCC	*Rlc1*^{Sp}*-GFP* and *Rlc1*^{Sj}*-GFP* assembly in *S. pombe*
PromRlc1Sp/Sp-REV	TTTTCCTTCGAAGAGAACATCGTTAACAGAGCAAATGATCAAA TAAG	*Rlc1*^{Sp}*-GFP* assembly in *S. pombe*
Rlc1Sp/Sp-GFP-FWD	GATCATTTGCTCTGTTAACGATGTTCTCTTCGAAGGAAAATTC CTTAGG	*Rlc1*^{Sp}*-GFP* assembly in *S. pombe*
Rlc1-GFP-PJK210-REV	CCACCGCGGTGGCGGCCGCTCTAGAACTAGTGGATCCCCCGCC GGTAGAGGTGTGGTCAATAAGAG	*Rlc1*^{Sp}*-GFP* and *Rlc1*^{Sj}*-GFP*

		assembly in *S. pombe*
PromRlc1Sp/Sj-REV	CGTTTGTTTTTTGAAGTCATCGTTAACAGAGCAAATGATCAAA TAAG	*Rlc1^{Sj}-GFP* assembly in *S. pombe*
Rlc1Sj/Sp-GFP-FWD	GATCATTTGCTCTGTTAACGATGACTTCAAAAAACAAACGTCT CCCTAAAAG	*Rlc1^{Sj}-GFP* assembly in *S. pombe*
Rlc1-S35A-FWD	T TCT CAA AGA GTT GCT GCC CAA GCC GCT AAA CGA GCA GCT TCT GGT GCA TTT GCG CAA CTT ACT TCT TCC CAA ATT CAA G	*Rlc1^{Sp}* serine-35 replaced by alanine (site-directed mutagenesis)
Rlc1-S35A-REV	CTTGAATTTGGGAAGAAGTAAGTTGCGCAAATGCACCAGAAG CTGCTCGTTTAGCGGCTTGGGCAGCAACTCTTTGAGAA	*Rlc1^{Sp}* serine-35 replaced by alanine (site-directed mutagenesis)
Rlc1-N23S-FWD	AAA AGC TTA CCG TCT AAA CTC GTC ACT TCA AAA CGA ATT TCC TCGGGAACATTTTCTCAATTAACAACCTCACAGATTCAG	*Rlc1^{Sj}* asparagine-23 replaced by alanine (site-directed mutagenesis)
Rlc1-N23S-REV	CTGAATCTGTGAGGTTGTTAATTGAGAAAATGTTCCCGAGGAA ATTCGTTTTGAAGTGACGAGTTTAGACGGTAAGCTTTT	*Rlc1^{Sj}* asparagine-23 replaced by alanine (site-directed mutagenesis)
Rlc1-S35D-FWD	T TCT CAA AGA GTT GCT GCC CAA GCC GCT AAA CGA GCA GAT TCT GGT GCA TTT GCG CAA CTT ACT TCT TCC CAA ATT CAA G	*Rlc1^{Sp}* serine-35 replaced by aspartic (site-directed mutagenesis)
Rlc1-S35D-REV	CTTGAATTTGGGAAGAAGTAAGTTGCGCAAATGCACCAGAAT CTGCTCGTTTAGCGGCTTGGGCAGCAACTCTTTGAGAA	*Rlc1^{Sp}* serine-35 replaced by aspartic (site-directed mutagenesis)
Rlc1-T104WT108W-FWD	ATAAATCCGCCTATTAATTTAGCCGCTTTTCTCTGGGCGATGG GTTGGATGCTGTGTCGAATCTCCCCC AGAAATGATCTA	*Rlc1^{Sp}* threonine-104 and threonine-108 replaced by tryptophan (site-directed mutagenesis)
Rlc1-T104WT108W-REV	TAGATCATTTCTGGGGGAGATTCGACACAGCATCCAACCCATC GCCCAGAGAAAAGCGGCTAAATTAATAGGCGGATTTAT	*Rlc1^{Sp}* threonine-104 and threonine-108 replaced by tryptophan (site-directed mutagenesis)
PromRlc1SpHelix-FWD	CGACGGTATCGATAAGCTTGATATCGAATTCCTGCAGCCCCAT ACTCCTTATTTCCTTCATTCCCAGC	*Rlc1(Δ19-33)^{Sp}-GFP* and *Rlc1(Δ19-33, S20A)^{Sp}-GFP* assembly in *S. pombe*
PromRlc1SpHelix-REV	GCAAATGCACCAGAAGATGCTGATGAAAATGGGGCACGTTTA GCAC	*Rlc1(Δ19-33)^{Sp}-GFP* and *Rlc1(Δ19-33, S20A)^{Sp}-GFP* assembly in *S. pombe*

Rlc1SpHelix-FWD	AACGTGCCCCATTTTCATCAGCATCTTCTGGTGCATTTGCGCAAC	*Rlc1(Δ19-33)^{Sp}-GFP and Rlc1(Δ19-33, S20A)^{Sp}-GFP* assembly in *S. pombe*
PromRlc1SjNterm-REV	TGCGCAAATGCACCAGAAGCAATTCGTTTTGAAGTGACGAGTTTAG	*Rlc1NtermSj^{Sp}-GFP* assembly in *S. pombe*
Rlc1(S35A)-GFP-FWD	TCGTCACTTCAAAACGAATTGCTTCTGGTGCATTTGCGCAACTTAC	*Rlc1NtermSj^{Sp}-GFP* assembly in *S. pombe*
Rlc1Sp-Seq-F	ATGACTTGCTGATATCCTCGC	*rlc1^{+Sp}* sequencing
Rlc1Sj-Seq-F	ATGGCTCTCTAACAAGCAACT	*rlc1^{+Sj}* sequencing